Ultimate moment capacity of bolted joint for cold-formed aluminium back-to-back channel sections

Zahid Hasan

Supervisors: Dr. Krishanu Roy **and** Dr. Bikram Paul

A thesis submitted in partial fulfilment of the requirements for the degree of Master of Engineering, The University of Waikato, 2026

ABSTRACT

Cold-formed aluminium (CFA) channel sections are gaining popularity in structural applications as a lightweight and corrosion-resistant alternative to carbon steel, especially in coastal and aggressive environments. However, their effective use depends critically on the performance of their connections. This research investigates the structural behaviour of bolted moment connections in back-to-back CFA channel sections. Key factors such as web buckling, shear lag, and bending shear interaction were identified as influencing the ultimate moment capacity of these joints.

An extensive numerical study of 1008 validated finite element (FE) models was conducted using ABAQUS. Moreover, validation was carried out based on experimental tests available in the literature. The Direct Strength Method (DSM) showed noticeable deviations from FE results in several cases, highlighting the limitations of DSM when applied to CFA sections. A parametric analysis was performed to examine the influence of cross-sectional size, thickness, web holes, and aluminium alloy grade and temper.

Based on these findings, a new predictive equation is proposed for the reduced moment capacity of CFA back-to-back channel sections. The equation was rigorously assessed for reliability and accuracy, and it provides a practical tool for engineers designing CFA portal frame connections.

Keywords: Bolted joints, Cold-formed aluminium, Moment capacity, Finite element modelling, Portal frames.

PREFACE

This thesis is submitted to the University of Waikato, New Zealand, in partial fulfillment of the requirements for a master's degree in civil engineering. The work presented here has not been submitted for any degree or diploma at any other institution. To the best of my knowledge, this thesis contains no material previously published or written by others, except where proper citation is provided.

ACKNOWLEDGEMENTS

First and foremost, I extend my deepest gratitude to my supervisors, Dr. Krishanu Roy, and Dr. Bikram Paul, for their unwavering support and guidance throughout my research journey. Their invaluable insights and mentorship have been instrumental in the successful completion of my thesis and have significantly contributed to my development as an independent researcher.

I am particularly grateful to Dr. Bikram Paul for his insightful feedback and assistance throughout the process. I also sincerely appreciate my well-wishers in New Zealand, whose encouragement has been vital in shaping this thesis.

My heartfelt appreciation goes to my family, my beloved wife Nurshad Jahan Mim, my mother Ferdushi Rahman, my father Mozibur Rahman, and my brother Rayhan Ferdous for their support and motivation throughout the year.

I would like to thank my friend Juwel Amin, Wosiqur Rahman Rafiq, and Gagan Singh for their unwavering support.

Lastly, I am grateful to the University of Waikato and the School of Engineering for providing the necessary computing resources.

NOTATION

Cold-Formed Aluminium	CFA
Cold-Formed Steel	CFS
Finite Element	FE
Back-To-Back	BTB
American Iron and Steel Institute	AISI
Australian and New Zealand Standards	AS/NZS
Finite Element	FE
Finite Element Analysis	FEA
Finite Element Modeling	FEM
Direct Strength Method	DSM
Cantilever length	$l$ca
Bolt group spacing	b_d
True stress	σt
True strain	εt
Engineering stress	σe
Engineering strain	εe
Young's modulus	E
Kilo-Newton	kN
Kilo-Newton Metre	kNm
Millimetres	mm

Metre	m
Newton per millimetre square	N/mm^2
Thickness	t
Yield stress	f_y
Ultimate stress	σ_u
Moment capacity from FEA	M_{FEA}
Moment capacity from DSM	M_{DSM}
Moment capacity from Existing equation ext.	$M_{\text{Existing equation ext.}}$
Yield moment	M_y
Nominal member moment capacity for lateral-torsional buckling	M_{be}
Nominal member moment capacity for local buckling	M_{bl}
Non-dimensional slenderness used to determine M_{bl}	λ_l
Nominal member moment capacity for distortional buckling	M_{bd}
Non-dimensional slenderness used to determine Mbd	λ_d
Elastic local buckling moment	M_{ol}
Elastic distortional buckling moment	M_{od}
Elastic critical moment for lateral-torsional buckling	M_{cr}
Ultimate moment capacity	M_u
M_u of channel-section as determined from BS5950: Part 5	M_u^{BS}

M_u from test	M_u^{EXP}
M_u from FEA	M_u^{FEA}
Length of bolt-group	a_b
Breadth of bolt-group	b_b
Depth of stiffener	d_s
Width of the triangular area of bolted side-plate,	a
Edge width of bolted side-plate,	b
Pitch of the frame	θ_a

Table of Contents

List of Figures

List of Tables

Chapter 1- Introduction

1.1 Background

In recent years, New Zealand's construction industry has increasingly turned to aluminium alloys, recognising them as a more sustainable and eco-friendly choice for modern building projects [1-8]. The growing adoption is due to aluminium's desirable qualities, including light weight, ease of installation, convenience in transportation, recyclability, good ductility, corrosion resistance, and an attractive natural look. For this reason, approximately 25% of the world's aluminium production is currently used in the construction sector [2]. In addition to reducing carbon dioxide emissions, structural aluminium alloys are fully recyclable, which has earned them the reputation of being the "green metal" [2 & 3].

Fig. 1.1 shows aluminium alloy sections used as load-bearing members in engineering applications.[38]

Cold-formed aluminium (CFA) portal frames are widely used for commercial, industrial, and agricultural buildings worldwide, including in New Zealand and Australia. Even though extruded aluminium profiles have been widely used in structural applications for a long time, recent studies show that cold-formed aluminium sections offer a more cost-effective alternative [8]. Bolted joints incorporating brackets connected to the web of channel sections are widely utilized in structural applications due to their economic efficiency and simplicity in assembly.

Despite their economy and ease of fabrication, the unconnected flanges in such joints can lead to undesirable effects, such as premature local buckling near the bolted joints at the column. This failure can result in collapse and may cause the design moment capacity to be overestimated by up to 40% [9]. The probable causes of this behaviour have been clearly discussed by Lim et al. [10], Phan et al. [11] and Mojtabaei et al. [12] for cold-formed steel (CFS). However, similar discussions for CFA structures are not available in the existing literature.

Although numerous experimental component tests on the moment capacity of bolted joints in CFS portal frames particularly at apex and eaves joints have been documented in the literature [16–23], similar studies for CFA frames are lacking. Consequently, no design equations have yet been proposed for predicting the reduced moment capacity of CFA members.

For CFS, McCrum et al. [9, 29] conducted portal frame tests and their results also highlighted that ignoring the reduction in moment capacity of the channel sections can result in premature failure. More recently, Paul et al. [30] proposed a method to account for it in practical design considerations. However, an accurate, practical equation to predict the reduced moment capacity of back-to-back channel sections, consistent with the method, is still lacking. Since design guidelines for predicting the reduced moment capacity of CFA are currently unavailable, this study aims to address this gap.

First, a finite element model (FEM) is developed for bolted joints of CFA back-to-back channel sections which is then validated against the experimental tests by Lim and Nethercot [13]. An extensive parametric study is then conducted, considering all practical aspects consistent with New Zealand standards. Using the results from the parametric study, a new equation is proposed to predict the reduced moment capacity of back-to-back channel sections.

1.2 Problem statement

In modern construction, both single channel and back-to-back CFA channel sections are gaining attention due to their lightweight, corrosion-resistant, and recyclable nature. However, the design of CFA channel sections remains complex compared to traditional steel structures. While previous studies have focused on CFS sections, the increasing use of CFA channel sections underestimates the need for further investigation into their behaviour and structural performance.

Currently, there are no established design guidelines for predicting the ultimate moment capacity of bolted CFA channel sections. This study is conducted using FE software with careful modelling and significant computational effort. Based on the analysis, a predictive equation has been developed to estimate the ultimate moment capacity of these sections.

1.3 Aim and scope of this research

Specific objectives of this work are listed below:

(i) This research focuses on developing nonlinear FE models to analyze the structural behaviour of CFA channel sections. Cross sectional dimensions and material properties are used as reported in the literature. Geometric imperfections are also considered. The accuracy of the FE models is then validated by comparing the predicted failure modes and ultimate moment capacities with experimental data.

(ii) The validated FE model will be applied to carry out a detailed parametric study. Factors such as web depth, thickness of the sections, bolt group spacing are considered while doing parametric study.

(iii) An equation has been developed for predicting the ultimate moment capacity of bolted joint back-to-back CFA channel sections.

1.4 Outline of the thesis

The thesis is structured into the following six chapters:

Chapter 1 presents a brief overview of the background, problem statement, aim and scope of the research, along with an outline of the thesis.

Chapter 2 provides a comprehensive review of prior studies on aluminium as structural material, aluminium channels, CFA channels, back-to-back CFA channel sections in portal frame, and back-to-back CFS channel sections in portal frame. The literature review on CFA reveals a lack of specific guidelines for determining the ultimate moment capacities of bolted joint of cold-formed aluminium for back-to-back channel sections. Furthermore, despite the growing use of CFA in industry, researchers have yet to develop a simplified method for determining their reduced moment capacity.

Chapter 3 offers a brief overview of the modelling technique used to develop the FE model. Additionally, the FE model was validated against the test results reported by Lim and Nethercot [13]. The moment capacity of the developed FE model closely matched the experimental results and is shown in Table 3-2. Additionally, a parametric investigation involving 1008 models is presented in this chapter. The study considered parameters including thicknesses ranging from 2.50 mm to 4.00 mm, web depths varying from 150 mm to 400 mm, and a_b/d ratio 0.5 to 2.5 for bolt group 2×2, 3×2 and 4×2. Based on the parameter studied, the effect of a_b/d, d/t and b_d/t on the reduced moment capacity are presented.

Chapter 4 compares the reduced moment capacities obtained from the DSM [64] [65] with FEA for CFA. Moreover, the comparative accuracy of different authors Lim and Nethercot [13], and Mojtabaei et al. [28] against finite element results for predicting the reduced moment capacity is also presented here. Finally, an equation is proposed, though there are some existing equations which have been widely applied in CFS connections, several limitations became evident when extended to CFA channel sections.

Chapter 5 provides a concise summary of the thesis, along with detailed conclusions based on the parametric study and the influence of various parameters. Furthermore, the chapter discusses potential future research directions related to this work.

Chapter 2- Literature Review

This chapter presents a detailed review of the existing literature on the behaviour of CFA back-to-back channel sections. The review covers aluminium as a structural material, aluminium channel sections, CFA channels, CFA back-to-back channel sections, and their application in portal frames. Previous studies on CFS back-to-back channel sections in portal frames are also reviewed, followed by the identification of research gaps and the formulation of research objectives. As a structural material, aluminium alloys are becoming more popular in structural applications because they are strong, lightweight, and naturally resistant to corrosion. They can also be shaped easily and recycled without losing quality. According to Georgantzia et al. [32], about 25% of all aluminium produced worldwide is now used in the construction sector. This growth is mainly due to the need for lighter structures and increasing pressure to build sustainably (Fig. 2.1). Unlike steel, aluminium can be extruded into complicated hollow sections. In addition, modern production methods have reduced the energy required to make aluminium by around 75% since 1995 [32]. Because it can be recycled and has a much lower environmental impact than before. Aluminium is now considered a truly “green” building material [32].

In structural engineering, aluminium has already been widely used particularly in applications where certain alloys can achieve strength levels close to those of steel. In recent years, considerable attention has been directed toward materials that can undergo large plastic deformations at relatively low strain levels, often referred to as low yield metals. In this context, pure aluminium presents a promising option [33]. The researchers have suggested using pure aluminium to fabricate shear panels that act as energy-dissipating dampers, offering passive seismic protection for both steel and reinforced concrete structures (Fig. 2.2).

Fig. 2.1 shows example of aluminium alloy structure [32]

Aluminium and its alloys have been available since the end of the 19th century [34]. One of the first major structural uses of aluminium was in the frames of the Schwarz and Zeppelin airships, which are considered the earliest 3D metal structures and early examples of lightweight aerospace design [34]. Even though these structures were built more than 100 years ago, their design was already quite advanced. Over time, aluminium became widely used in transport systems such as aircraft, ships, trains, and vehicles and in pressure vessels like tanks, silos, and industrial domes [34].

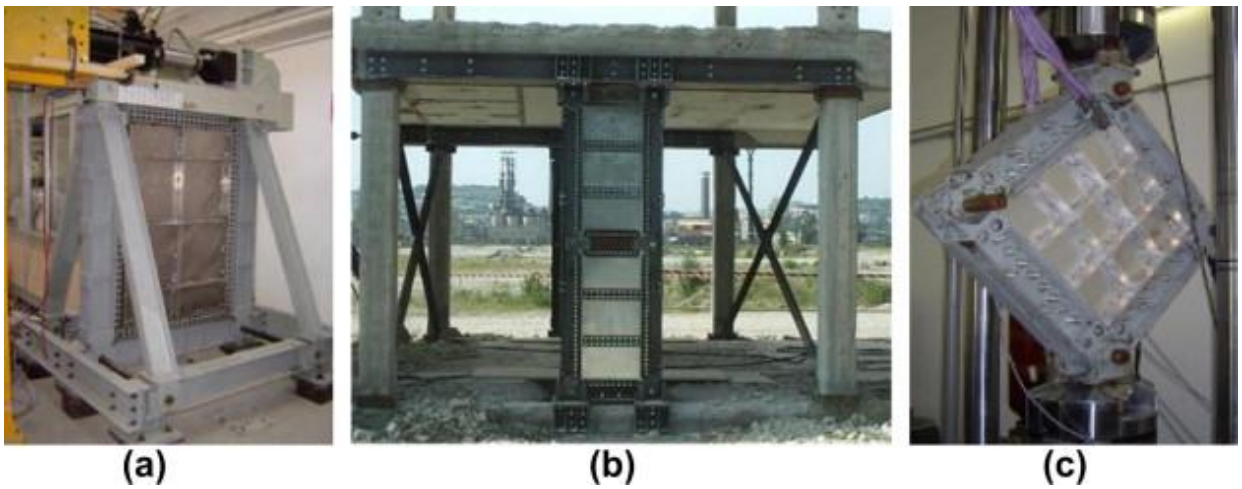

Fig. 2.2 shows (a) Steel and reinforced concrete (b) frames equipped with infill pure aluminium shear panels; (c) pure aluminium shear panel arranged in a bracing type configuration subjected to diagonal tension compression [33]

Its use later expanded to include large architectural roofs, including well-known buildings like the Glasgow Conference Centre and Lord's Cricket Ground in London. In 1951, Dome of Discovery was the largest aluminium dome in the world and marking the beginning of several major aluminium dome structures across Europe [34].

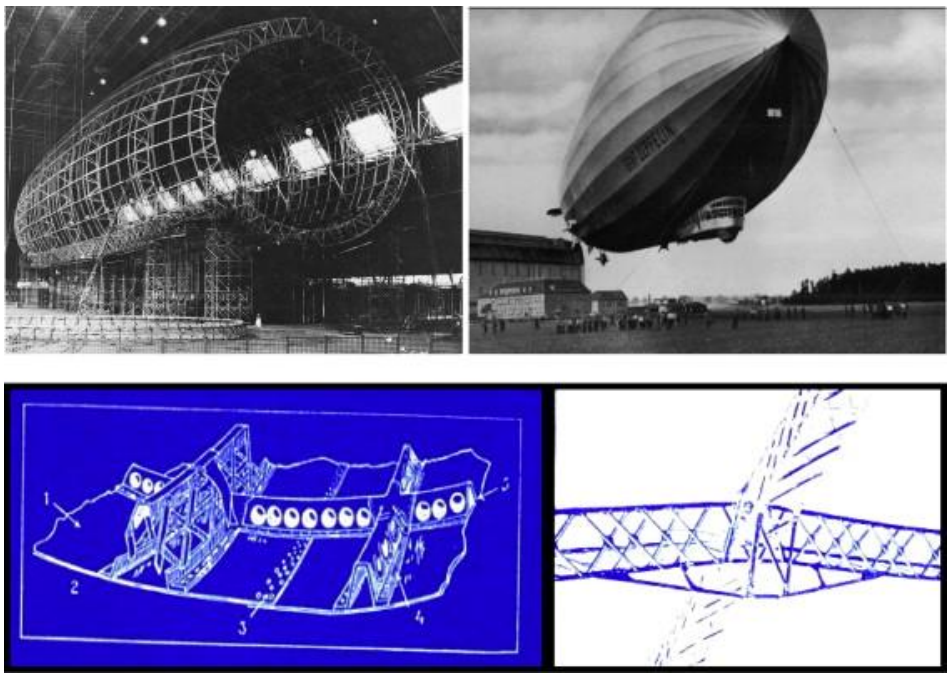

Fig. 2.3 shows aluminium structure of a dirigible and its structural details. [34]

Fig. 2.4 shows structure of a railway or metro car. [34]

Fig. 2.5 shows example of aluminium silos. [34]

Fig. 2.6 shows applications of aluminium roofing in UK [34]

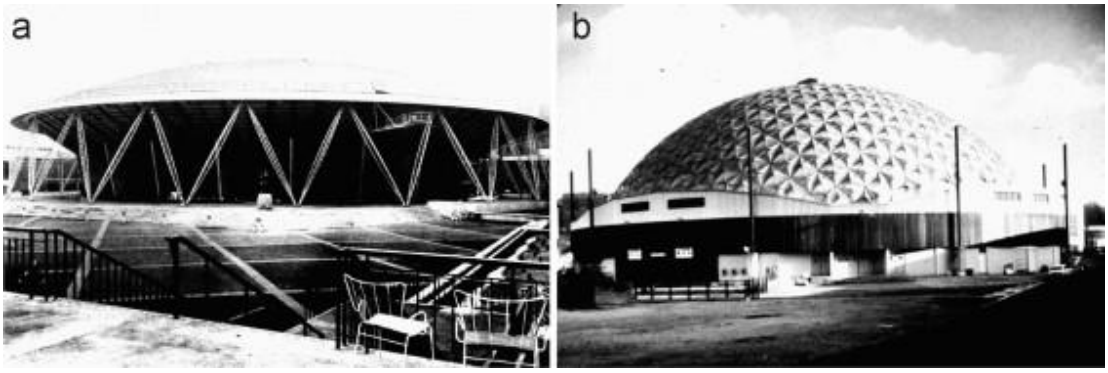

Fig. 2.7 shows First aluminium domes [34]

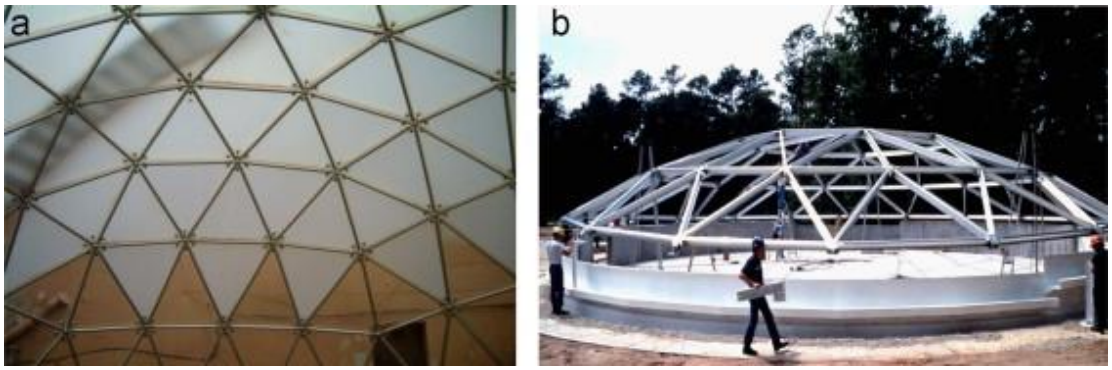

Fig. 2.8 shows different systems for building aluminium domes [34]

Fig. 2.9 shows two twin aluminium domes erected in the ENEL thermo-electrical power plant of Torrevaldaliga Nord (Civitavecchia, Italy) [34]

Following the recognition of aluminium as a viable structural material, research attention has shifted toward its use in practical member forms, particularly channel sections, which have been widely studied in recent years. Zhu et al. [35] investigated the bending behaviour of aluminium channel beams. Both plain and lipped channels made from 6063-T5 and 6061-T6 alloys using four-point bending tests were examined. Subsequently, finite element modelling was used to confirm the results. Their findings showed that most plain channels fail by local buckling when bent about the minor axis. On the other hand, lipped channels can experience both local and distortional buckling, especially in major axis bending.

Additionally, Georgantzia et al. [36] investigated how aluminium channel sections behave when loaded about their minor axis. Their study included 14 four-point bending tests on 6082-T6 aluminium channels with different dimensions and bending orientations. The results showed that specimens loaded with the web in compression mainly failed by yielding, while those loaded with the flange tips in compression experienced local buckling at lower curvature levels. After validating a detailed finite element model, the authors ran 140 parametric simulations covering different alloy types, aspect ratios, and slenderness values. This paper is significant because it provides rare experimental data and improved design rules for aluminium C-sections, which are increasingly used in lightweight building systems.

Moreover, Yuan and Zhang [37] carried out a detailed numerical investigation on aluminium alloy channel sections under minor-axis bending. They used validated finite element models based on existing experimental data. A large parametric study was completed and 468 FE models with different flange and web slenderness ratios, alloys (6082-T6 and 6063-T5), and bending orientations were conducted. This research confirms that conventional design rules are conservative for aluminium

channel sections and supports the need for improved design methods based on realistic buckling and inelastic behaviour.

Fig. 2.10 shows extruded aluminium alloy channel members [37]

Aluminium alloys can be easily extruded into many different shapes, including hollow profiles, channel sections, and stiffened forms. Channel sections are commonly used as rafters in lightweight roofs, wall studs in building frames, girts and mullions in curtain wall systems, and as chord members in roof trusses [37]. Figure 2.10 shows an example where extruded aluminium channel sections are used as columns in a structural system [37].

For high-strength aluminium alloy channel sections Sun et al. [38] carried out a large numerical study. Their focus was on the web crippling behaviour of high-strength aluminium alloy channel sections. Two advanced alloys, AA-6086 and 7075-T6 were analysed and 1024 finite element models were conducted for different web slenderness ratios, corner radii, bearing lengths, and lip configurations.

Another study focusing specifically on aluminium channel sections was carried out by Jiang et al. [39], who investigated the tensile performance of channels connected to gusset plates using both experiments

and numerical modelling. A total of nineteen specimens with either web bolted or flange bolted connections were tested, and the results were used to validate detailed finite element simulations. The authors showed that connection configuration and shear lag effects had a significant influence on strength and often reduce the effective capacity of the member.

While many studies have examined aluminium channel members, some studies have focused on cold-formed aluminium channels, which exhibit different material behaviour and structural performance due to the forming process. Huynh et al. [40] investigated the mechanical properties and residual stresses in cold-rolled aluminium channel sections made from 5052-H36 alloy. A total of 227 coupon tests were carried out, including flat and corner tensile tests, compression tests, and residual stress measurements on three different C-section sizes. The authors indicated the need for improved design provisions for cold-rolled aluminium channels.

McIntosh et al. [41] conducted a comparative study on the web crippling behaviour of cold-formed aluminium channel sections, carbon steel, and stainless steel under concentrated loading. A combination of experimental testing, numerical modelling, and reliability-based evaluation of current design rules was performed. The results showed that aluminium channels exhibited lower web crippling strength than steel sections because of their lower elastic modulus and different strain hardening characteristics.

Another study by Paul et al. [42] carried out the first combined experimental and numerical study on cold-formed aluminium channel beams with web holes under pure bending. The results showed that increasing hole diameter reduced the moment capacity by up to 18%. Following this, another key study by Pham et al. [43] showed that cold-rolled aluminium channel beams mainly fail by flexural-torsional buckling, and current specifications do not accurately predict their capacity.

Fig. 2.11 shows Cold-rolled aluminium C- and Z-sections [51]

In Part I, Pham et al. [44] carried out the first major experimental study on cold-rolled aluminium channel columns and examined how they fail under compression. Their results showed that current design standards are safe for short sections but can overestimate the strength of slender columns. Because existing rules were mostly developed for extruded aluminium, they do not correctly predict the behaviour of cold-rolled channel members. This study therefore highlights the need to update design methods for cold-rolled aluminium columns. Additionally, Pham et al. [45] extended the work by developing validated finite element models and carrying out a wide parametric study in Part II. Based on the parametric results, the authors proposed new Direct Strength Method equations that achieved the required reliability levels and provided a more accurate basis for designing cold-rolled aluminium channel columns.

Fang et al. [46] conducted a study using an XGBoost machine learning model to predict the web-crippling behaviour of perforated roll-formed aluminium alloy unlipped channels under interior-two-flange loading. They trained the XGBoost model using 1,080 FE-generated data points and 30 tests,

achieving 94% accuracy. Fang et al. [46] found that current design standards (AISI, AS/NZS, Eurocode) do not reliably predict web-crippling strength for perforated sections.

Fang et al. [47] conducted a study to examine how aluminium alloy back-to-back channel sections with web holes behave under axial compression. They tested fourteen screw-fastened stub and short columns and characterised the material properties and geometric imperfections. A nonlinear FE model was developed. After validating the model, they conducted 720 simulations to study how variables such as hole size, screw spacing, thickness, and column length affect the behaviour. When the results were compared with AS/NZS 4600 and AISI design provisions, both standards were found to be conservative by roughly 10%. Using the numerical results, Fang et al. proposed new axial strength reduction equations for back-to-back channels with web holes, and reliability analysis confirmed that the proposed formulas offer accurate strength predictions.

Similarly, Roy et al. [48] studied the axial behaviour of back-to-back built-up aluminium alloy channel sections because these members are increasingly used in lightweight structures where higher compression strength is needed. They conducted 15 compression tests and 232 FE simulations to evaluate the axial strength of back-to-back built-up aluminium channel section columns. When the results were compared with major design standards, most were conservative by about 20%, while ADM, AISI and AS/NZS 4600:2018 gave the most accurate predictions.

Moreover, Roy et al. [49] investigated the axial capacity of screw-fastened back-to-back aluminium channel columns by testing 12 specimens and running 246 FE models. Their results showed that AISI 2016 and AS/NZS 4600:2018 predict column strength accurately, while ADM 2020 and Eurocode 9 are overly conservative.

Having reviewed the behaviour of individual cold-formed aluminium channel sections, it is now important to consider how these sections perform within complete structural systems such as portal frames. Cold-formed aluminium is increasingly used in portal frames because it is lightweight, corrosion-resistant, easy to assemble, and capable of forming efficient thin-walled sections, making it ideal for modular and light-duty structural applications. In a major contribution to the field, Pham [50] examined the structural performance of cold-rolled aluminium portal frames formed from back-to-back lipped channel sections through full-scale testing and advanced numerical modelling. Pham's [50] research demonstrated that cold-rolled aluminium portal frames can be reliably designed using DSM, which more accurately predicts structural behaviour and ultimate strength than current aluminium standards.

Moreover, Nguyen et al. [51] conducted a series of four full-scale tests on long-span cold-rolled aluminium portal frames constructed from back-to-back built-up channel sections. Their main aim was to understand system behaviour and strategies for increasing ultimate strength. The authors also investigated structural enhancements, including rafter ties, modified apex connections, and sleeve stiffeners. Overall, the results demonstrated that column bracing and sleeve stiffener strengthening are crucial to the performance of cold-rolled aluminium portal frames.

While Nguyen et al. [51] focused on ultimate strength, Liu et al. [52] examined joint behaviour. Liu et al. [52] performed a combined experimental and numerical investigation to evaluate the flexural behaviour of apex joints in aluminium alloy portal frames, focusing on joints formed using rectangular hollow beams connected by double clamping plates. The authors developed a practical equation to predict the flexural capacity of aluminium alloy portal frame apex joints, combining the strength contributions of the clamping plates, the beam's effective net section, and the bolt group to give a realistic estimate of overall joint performance.

Following earlier work on ultimate strength, Nguyen et al. [53] conducted experimental and numerical investigations on the column base connections of portal frames constructed from cold-rolled aluminium built-up sections. This was the first detailed study on cold-rolled aluminium portal frame base connections and demonstrated that thicker and U-shaped brackets substantially increase flexural stiffness, while thinner brackets experience large deformation and localised failure.

After reviewing the available research on cold-formed aluminium (CFA) channel sections, the next section examines cold-formed steel (CFS) channel sections. In the CFA literature, no experimental tests using bolted back-to-back channels for the apex joint have been reported. However, in CFS research several papers have addressed this connection behaviour. Lim [54] conducted a study on apex joints and other bolted moment connections in cold-formed steel (CFS) portal frames, demonstrating that joint capacity has a significant influence on the overall performance of the frame. Moreover, Lim and Nethercot [13] studied bolted moment connections in cold-formed steel and found that the joints can be weaker than the members they connect because the web tends to buckle around the bolts. By testing real specimens and running FE models, they also found that, in practical joints, the moment capacity can be up to 20% lower than that of the connected sections. In this study, the FE model validation is performed using experimental test results reported by Lim and Nethercot [13].

In addition, Paul et al. [55] examined the apex joint of a cold-formed steel nested tapered box beam (NTBB) portal frame. At the apex, the beams are connected by bolted side-plates, and the study focused on the strength of these plates. The authors developed a non-linear elastoplastic FE model and carried out a large parametric study with 340 FE simulations. Based on the results, they proposed a design recommendation for the minimum required thickness of bolted side-plates to ensure adequate moment capacity. In another study, Paul et al. [56] stated that traditional welded or bolted end-plate joints in CFS portal frames can be costly and prone to cracking, and they proposed a bolted-side plate system

as a more efficient alternative that improves joint performance. Their study looks at improving joints in cold-formed steel (CFS) portal frames that use nested tapered box beam (NTBB) sections. The study showed that the bolted-side plate system can increase frame capacity by about 9%.

Besides, Stratan et al. [57] studied pitched-roof cold-formed steel portal frames made from back-to-back channel sections with bolted joints. They found that joints with bolts only in the web had reduced moment capacity and were more likely to buckle. Using the component method, they assessed joint stiffness and strength, and full-scale frame tests showed that their analytical predictions were reliable.

Recently, Paul et al. [30] highlighted that cold-formed steel (CFS) portal frames made from back-to-back channel sections are often incorrectly designed because engineers assume the joints are fully rigid and ignore shear lag effects. These simplifications can lead to unsafe designs by underestimating frame deflection and apex moments, while overestimating column strength. Based on this analysis, they proposed a simple beam-idealisation method that allows engineers to predict frame capacity more accurately.

After reviewing the available literature on CFA and CFS channel sections, it is evident that no studies have specifically addressed the prediction of the ultimate moment capacity of back-to-back CFA channel sections, particularly at bolted joint configurations, whereas several studies exist for equivalent CFS connections. Existing studies on CFA focus on overall frame behaviour, axial capacity, base connections, and apex joints. Despite the growing use of CFA channel sections in portal frames particularly in corrosive or coastal environments, it is observed that back-to-back CFA channels connected with bolted brackets often experience premature web buckling near the joints, reducing their effective moment capacity and compromising frame performance. The absence of experimental and numerical studies on this critical failure mechanism leaves engineers without reliable design guidance

and creates uncertainty in the safe and efficient use of CFA channel sections in portal frame construction.

Although much of the CFA literature does not address bolted joint moment capacity, similar issues have been explored in CFS research. Lim and Nethercot [13] examined the behaviour and moment capacity of bolted moment connections in cold-formed steel members. Their work is relevant to my study; however, the key distinction is that my research focuses on CFA channel sections rather than CFS. Although their study focused on CFS, the experimental results from Lim and Nethercot [13] offer a suitable benchmark for validating the present model due to the similarity in joint configuration.

One of the primary objectives of this study is to address the lack of design guidance for predicting the ultimate moment capacity of bolted CFA channel sections. This is done using advanced finite element modelling. From the validated results, a new prediction equation is developed, and a reliability analysis is carried out to confirm that the proposed equation is safe and suitable for future design use.

Chapter 3- Development of Finite Element Model

3.1 Introduction

As defined in AS/NZS 4600 (2018), advanced analysis considers material and geometric nonlinearity, as well as imperfections, to provide a realistic design method for steel structures with compact cross-sections. For aluminium, the relevant international standard is usually Eurocode 9 [58] and Aluminium Design Manual [59]. However, CFA is becoming popular as they are lightweight, corrosion-resistant, and have a high strength-to-weight ratio, but their lower stiffness and higher sensitivity to local buckling make their behaviour different from cold-formed steel. Unlike extruded aluminium sections, cold-forming allows the production of thin-walled profiles that use material more efficiently. However, this benefit also comes with challenges, as thinner sections are more vulnerable to both local and global instabilities.

For advanced analysis, the development of a robust FE model is essential to predict the behaviour of CFA channel sections. When developing the finite element models, both local and distortional buckling were considered as potential failure modes. With respect to local and distortional buckling, aluminium alloys are more prone than steel. The modelling and testing of bolted joints in CFS members has already been thoroughly investigated. Both laboratory experiments and FE analyses have been used to study their ultimate moment capacity, failure modes, and the influence of factors such as web buckling and bolt-group configurations [54, 60, 61]. In accordance with these studies, FE models may accurately represent data from experiments when fully validated, which makes them a reliable resource for parametric research and for developing design recommendations.

Apex joints and other bolted moment connections in CFS portal frames were examined in previous work by Lim [54], which showed the significance of joint capacity in overall frame performance.

Although the flexural strength of CFA members has been studied, the behaviour and moment capacity of bolted apex joints in CFA back-to-back channel sections remain underexplored.

Following Lim and Nethercot [13], a similar modelling approach has been applied in this thesis to CFA sections. Even though aluminium differs from steel, established CFS methods using experimental validation and FE modelling have been successfully adapted for CFA joint studies.

In this chapter, the process followed to develop a finite element model capable of simulating the behaviour of bolted joints in CFA back-to-back channel sections has been described. The finite element program ABAQUS [62] was employed to model the apex joint of CFA portal frames using back-to-back channel sections. In addition, the ultimate moment capacity of bolted joints in CFA back-to-back channel sections was investigated through the use of ABAQUS [62]. The FE models developed in this study were validated against the closest experimental tests that had been conducted by Lim and Nethercot [13].

3.2 **Descriptions of reference test for bolted joint after Lim and Nethercot** [13]

No experimental tests using bolted back-to-back channels for the apex joint have been reported in the literature for aluminium. Lim and Nethercot [13] described apex joint tests for cold-formed steel using the arrangement depicted in Fig. 3.1. This section briefly describes the closest experimental tests to bolted back-to-back channels in the literature, and these tests are used to validate the FE modelling.
Fig. 3.1 depicts the boundary conditions, lateral restraints, and loads in detail. As shown in Fig. 3.2, apex joint tests described by Lim and Nethercot [13] were performed under pure bending. The maximum distance between the points of lateral restraint for each tested apex joint was ensured to not exceed the maximum unrestrained distance of 1365 mm. The observed failures were governed by premature buckling of the apex joint, while no evidence of lateral-torsional buckling was noticed, as

adequate lateral restraints had been provided. The measured dimension of the channels tested is shown in Fig. 3.3 and Fig. 3.4 describes the loading idealization applied to the brackets and provides the details of the apex brackets are tabulated in Table-1 and the value of θ_a (pitch of the frame) is 10◦.

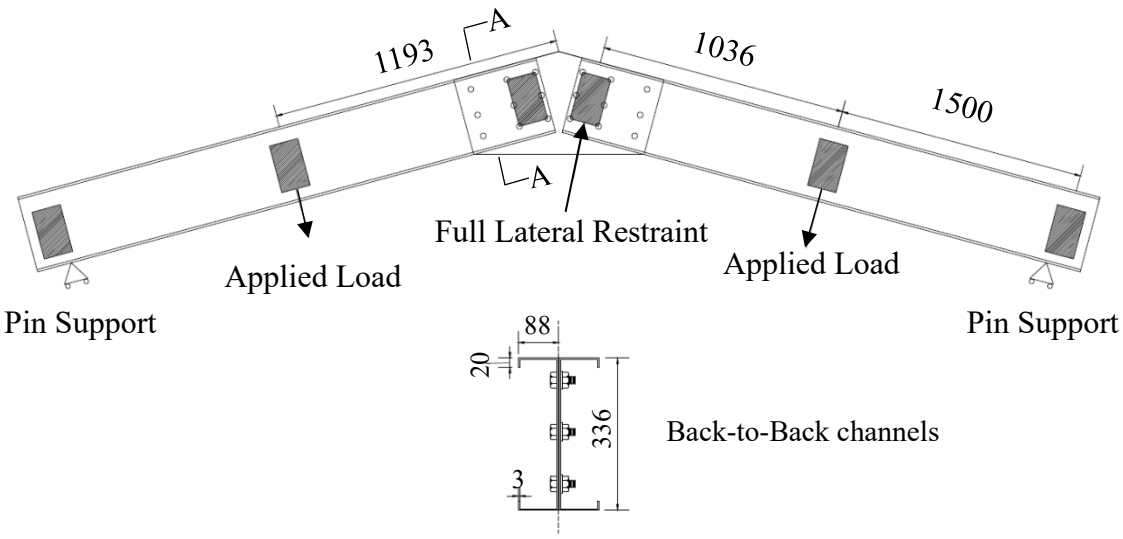

Fig. 3.1 Details of apex joint test (dimensions in millimeters)

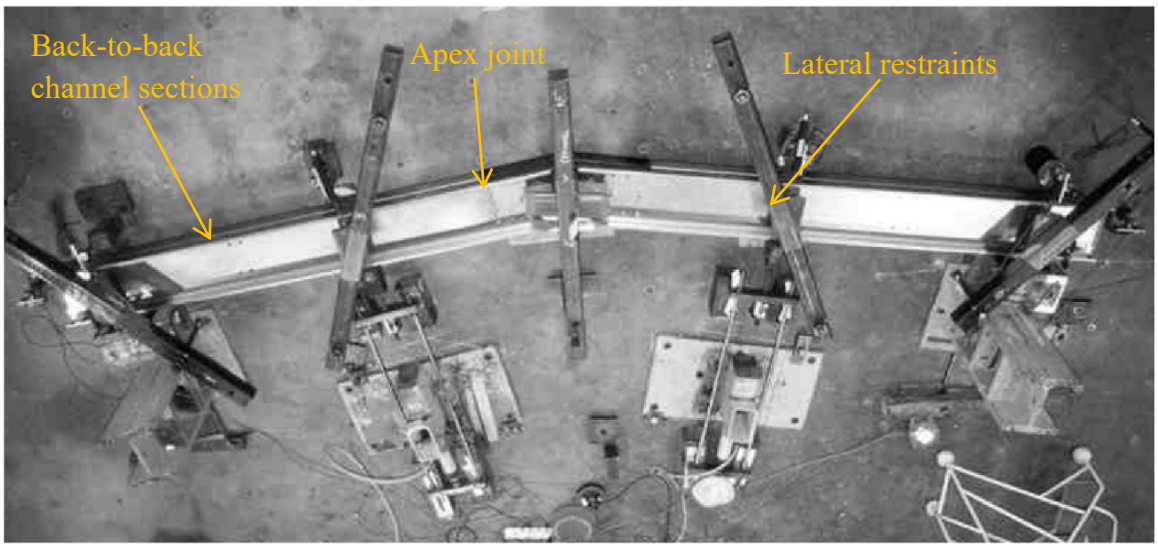

Fig. 3.2 Photograph of laboratory test of apex joint [54]

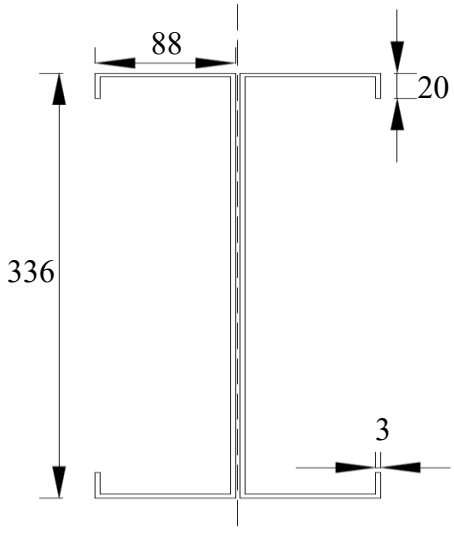

Fig. 3.3 Dimensions of the back-to-back channel (dimensions in millimeters).

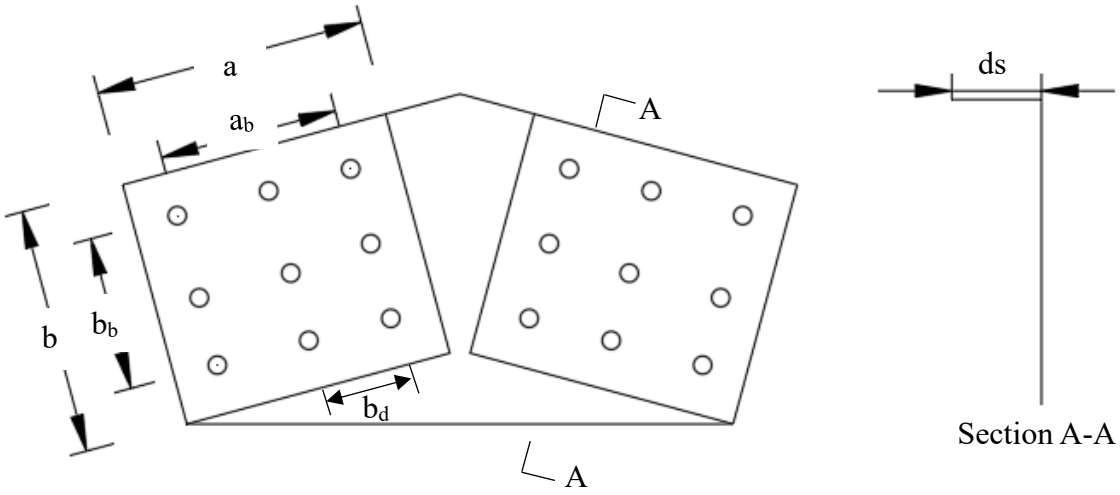

Fig. 3.4 Parameters showing the bracket details

Table 3-1 Dimension of apex brackets and bolt groups

Tests	a	b	t	a_b	b_b
	mm	mm	mm	mm	mm
A	525	340	3.98	315	230
B	600	340	3.98	390	230
C	675	340	3.98	465	230
D	825	340	3.98	615	230

3.3 FE Modelling Technique

The modelling process commenced with the creation of the channel geometry as individual parts. Compared with steel, aluminium exhibits a lower elastic modulus and a gradual yielding response without a distinct yield point. Consequently, aluminium members do not display an abrupt onset of plastic deformation and demonstrate increased sensitivity to local buckling.Its material properties are carefully defined using both elastic and plastic parameters. To accurately represent the thin-walled

nature of the sections, shell elements are used, as they are well suited for capturing local instabilities. The modelling techniques are described in this section.

3.4 Geometry Modelling of Channel Sections

The FE idealisation shown in Figure 3.6 illustrates the modelling approach adopted to simulate the experimental test setup of Lim and Nethercot [13]. According to Lim and Nethercot [13], modelling only one channel instead of a full back-to-back pair directly affects how stresses distribute across the joint web and flanges. The back-to-back arrangement provides torsional and lateral restraint, helping the two webs share load and limit out-of-plane deformation. When only one channel is used, that restraint is lost, and the section becomes more flexible. This simplification leads to a non-uniform stress distribution. Concentrated bolt forces transfer through a single web, creating localized web bending and compression flange buckling near the bolt group and as observed in the experimental test of Lim and Nethercot [13].

On the other hand, a full back-to-back pair would distribute these stresses more evenly between the two webs, lowering local stress intensity and deflection. Because the single-channel model overpredicts deformation and stress for the same applied moment. Therefore, this modelling choice is conservative. It underestimates stiffness and strength, giving a safe lower-bound prediction of the joint's moment capacity. As can be seen, the idealization consists of only a single channel-section loaded under pure bending. Such an arrangement is justified as it was the channel-sections that failed in the laboratory tests [13]. This is also a reason for not modelling the full experimental test setup. Instead, a single channel with a cantilever length $l$ca is modelled. In this model, the value of $l$ca is taken as four times the web depth, giving a length of 1344 mm.

3.5 Element and material

The S4R element, which is a 4-noded quadrilateral flat shell element with reduced integration, was used from the ABAQUS [62] library. A mesh sensitivity analysis was conducted to determine the suitable mesh size (See Fig. 3.5). It is found that the mesh size of 5 mm × 5 mm is appropriate to use in this study. As shown in Fig. 3.6, the bolted channel section was found modelling with a mesh size of 5 mm × 5 mm. Material nonlinearity was incorporated in the finite element models to accurately capture the post-yield behaviour of cold-formed aluminium members. By including material nonlinearity, the numerical analysis is able to represent the interaction between yielding and buckling in thin-walled channel sections, providing a more realistic prediction of joint behaviour.

The simulated material behaviour follows an elastic-perfectly plastic model. Although aluminium alloys exhibit non-linear strain hardening which means that after yielding, stress does not increase at a constant rate with strain; instead, the stress strain curve becomes curved. Non-linear strain hardening affects the post-yield deformation of aluminium members. This post-yield behaviour refers to the material response after yielding, characterised by plastic deformation and strain-hardening effects. Post-yield behaviour influences how much extra strength and deformation a member can sustain after yielding, but in cold-formed aluminium members, failure usually occurs by buckling before this post-yield behaviour has time to develop. However, an elastic-perfectly plastic model is sufficient for CFA joint analysis because the governing failure mode is local buckling rather than material yielding. The elastic-perfectly plastic model correctly identifies the point at which the material first starts to yield and provides conservative moment capacity predictions. For this reason, an elastic-perfectly plastic model is chosen. The elastic modulus represents the stiffness of a material in the elastic range and defines the relationship between stress and elastic strain. Aluminium alloys have a lower elastic modulus, approximately 68,000 N/mm², compared with about 200,000 N/mm² for structural steel. This lower elastic modulus leads to reduced initial stiffness and larger elastic deformations under the same

loading conditions. In CFA members, the elastic modulus remains essentially unchanged across commonly used tempers, such as H-36 and H-38, even though these tempers exhibit significant differences in yield and ultimate strength. The yield stresses of channel section and elastic modulus (E) are presented in Table 3-3.

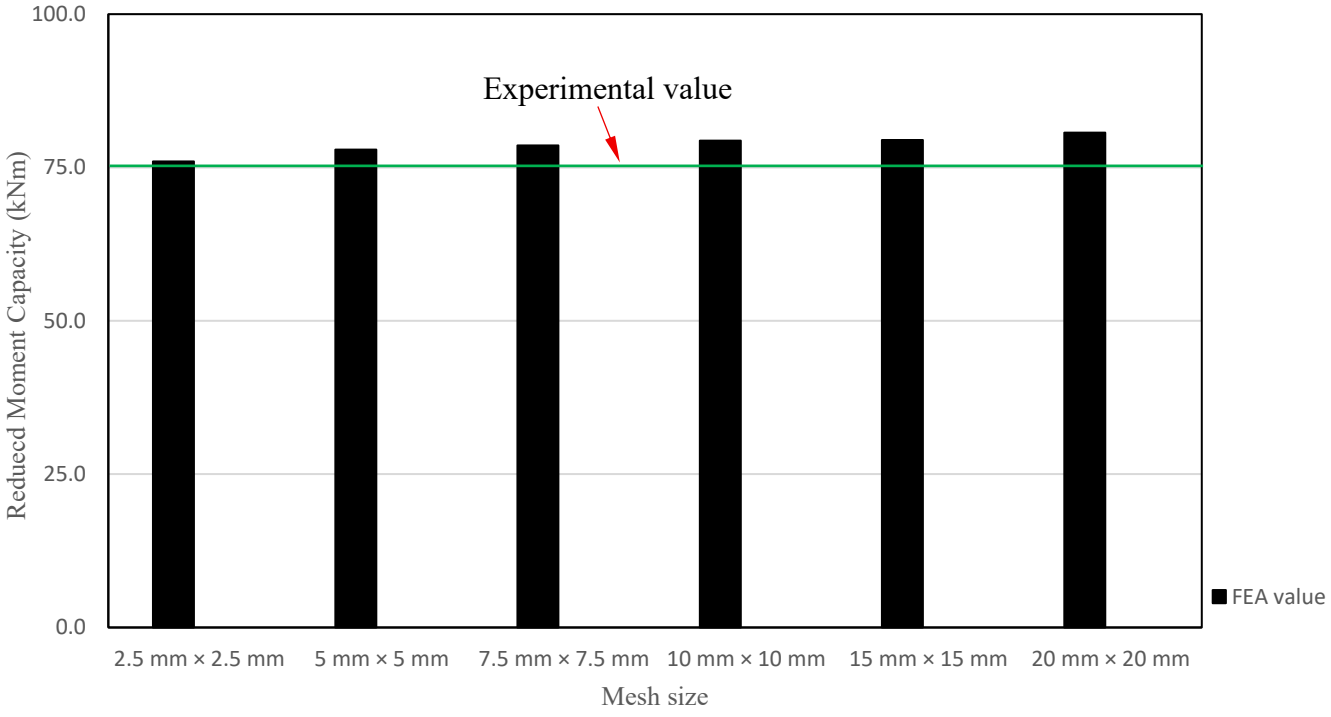

Fig. 3.5 Mesh sensitivity analysis results

3.6 Contact and connection

As only a single channel is modelled (Fig. 3.6), the behaviour of the bolted joints is idealised using the SPRING1 element in ABAQUS [62]. Detailed bolt modelling is not used because the main purpose of this study is to understand the overall joint and member behaviour, not the behaviour of individual bolts. In this study, the ultimate moment capacity is governed mainly by buckling of the thin-walled aluminium sections, rather than bolt failure. Therefore, simplified bolt modelling is

sufficient to capture the global joint stiffness, load transfer, and failure trends. In addition, similar simplifications are also used in CFS joint studies [13]. One end of the spring is grounded, while the other end is connected to the nodes of the channel section. The SPRING1 element is ideal for buckling analysis because it provides a simple, linear elastic restraint. Since only one channel is modelled, surface contact need not be defined. The stiffness value used for the spring element was 10 kN/mm [13] and previous study [68] has shown that this value is reasonable. A brief sensitivity check, in which the spring stiffness was increased and decreased about this value, showed no material change in the predicted ultimate moment capacity or failure mode, confirming that the response is governed by buckling instability rather than by the assumed spring stiffness. In this modelling approach, bolt slip is not considered. The elastic spring elements assume that the bolts are already in full contact with the plates, so the effect of bolt slip is ignored. This is reasonable for the present study because the joint behaviour and ultimate capacity are controlled by buckling.

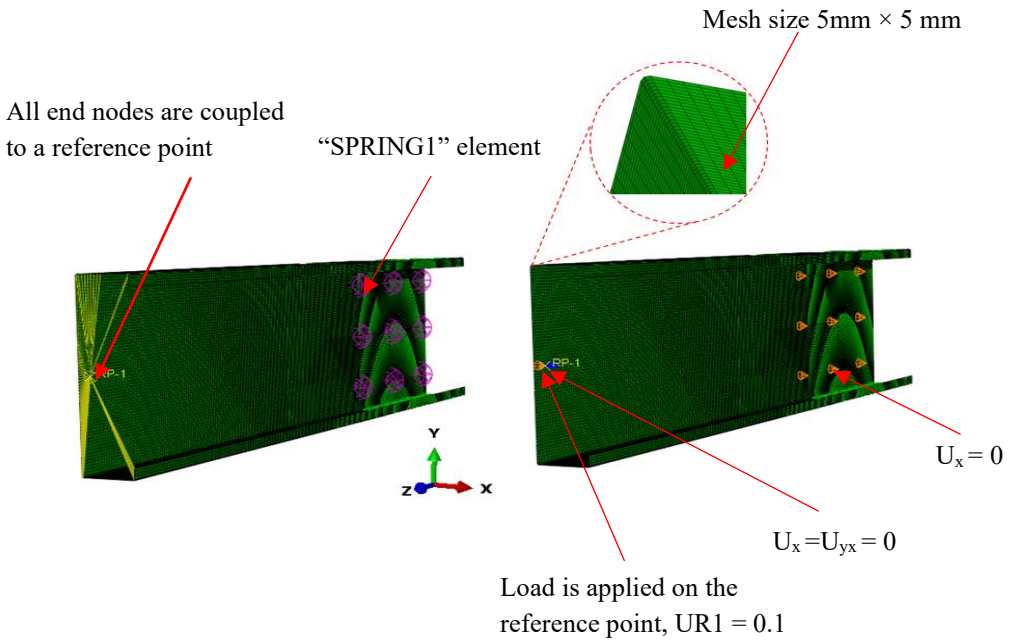

(a) Springs and coupling (b) Boundary condition and

Fig. 3.6 Details of the FE model

3.7 Imperfections in CFA Sections

In the study by Lim and Nethercot [13], lateral-torsional buckling was restrained by a dedicated bracing system, which meant that all specimens ultimately failed through cross-sectional instabilities close to the connection. Hence, depending on which buckling mode had the lower critical buckling stress, either a local or a distortional buckling imperfection was added to the model. Using the scaled first eigenmode as the shape of the initial imperfection, an elastic buckling analysis of the apex connection was performed in ABAQUS to accomplish this. The amplitude of the imperfection was determined based on the work by Schafer and Peköz [63] whereby the 50% value of the cumulative distribution function of the imperfection magnitudes was chosen. The magnitudes of the local and distortional imperfections, respectively, are 0.34t and 0.94t, and this is the most likely imperfection. Imperfection magnitudes were taken as per the recommendations of AS/NZS 4600 [64].

3.8 Boundary conditions and loading

Figure 3.6b shows the boundary conditions and loading employed in the FE model for this study. As illustrated, rather than replicating the entire experimental setup, the modelling was simplified by representing only a single channel. In this simplified FE model, the nodes at the ends of the channel section were coupled to a reference point located at the centroid of the section, which was subjected to an opening moment. At this reference point, both out-of-plane rotation and lateral translation were restrained (Fig. 3.6b).

3.9 Validation of the finite element model

Before applying the developed FE model to CFA sections, its accuracy needed to be verified. To do this, the model was benchmarked against experimental results from Lim and Nethercot [13], who tested apex joints in CFS portal frames. Table 3.2 presents the results of the nonlinear analysis of the apex

joint. The predicted failure load closely matched the experimental data, with a standard deviation of 0.04 and an average percentage difference of 0.25%.

This close alignment provides strong evidence that the FE model is capable of capturing the complex interaction of geometric nonlinearity, local buckling, and semi-rigid joint behaviour that governs the performance of apex joints. Validating the model against trusted experimental work was a critical step, as it confirms that the same modelling approach can now be extended with confidence to cold-formed aluminium back-to-back channel sections. By establishing this reliability, the present study builds a robust foundation for carrying out more detailed parametric analyses and ultimately developing new design recommendations for CFA joints. Furthermore, no published studies were identified that experimentally or numerically investigate the ultimate moment capacity of back-to-back CFA channel sections at the apex joint. This approach is considered reasonable because the joint response is largely governed by thin-walled geometry, bolt configuration, and buckling-dominated behaviour, which are common to both CFA and CFS systems. Lim and Nethercot [13] have been widely cited and adopted in subsequent thin-walled steel research, making it a credible and well-accepted benchmark for evaluating joint behaviour in related thin-walled structural systems.

Moreover, the buckling failure of the channel section matches the experimental results from Lim and Nethercot [13], as shown in Fig. 3.7, suggesting the modelling techniques adopted here can be used for further study. Buckling dominated failure allows the validation to be transferable because the failure is controlled by elastic instability, which depends mainly on the member's geometry, support conditions, and stiffness. Buckling-based validation does not capture post-yield material effects, such as aluminium strain hardening, or local connection behaviours, such as bolt bearing deformation, because failure occurs before developing these mechanisms.

Table 3-2 Comparison of experimental and FEA results of apex joint tests after from Lim and Nethercot [13]

Test	a_b	$\frac{a_b}{D}$	b_b	t	f_y	M_u^{EXP}	M_u^{FEA}	$\frac{M_u^{FEA}}{M_u^{EXP}}$	Failure mode
	mm		mm		N/mm^2	kNm	kNm		
A	315.00	0.94	230.00	2.98	358.00	75.00	77.90	0.96	
B	390.00	1.16	230.00	2.98	358.00	77.50	78.90	0.98	Local buckling to the web adjacent to the bolt group
C	465.00	1.38	230.00	2.98	358.00	82.50	80.50	1.02	
D	615.00	1.83	230.00	2.98	358.00	87.50	83.40	1.05	
							Average	1.01	
							Standard Deviation	0.04	

The modelling approach in this study follows the methods proposed by Schafer and Peköz [63], who developed detailed guidelines for simulating imperfections and residual stresses in cold-formed thin-walled members. Their work supports using eigenmode-based geometric imperfections derived from linear buckling analysis to represent realistic initial deviations. They also highlighted the need for imperfection sensitivity studies, showing that strength varies with imperfection size and distribution. Although their data were based on steel, the same modelling principles apply to aluminium members. Therefore, this study adopts their approach in ABAQUS [62] to ensure a validated and reliable representation of geometric imperfections.

It is emphasised that in the experimental tests described by Lim and Nethercot [13], the apex joints were tested under four-point bending. Therefore, only failure loads are reported in the present study.

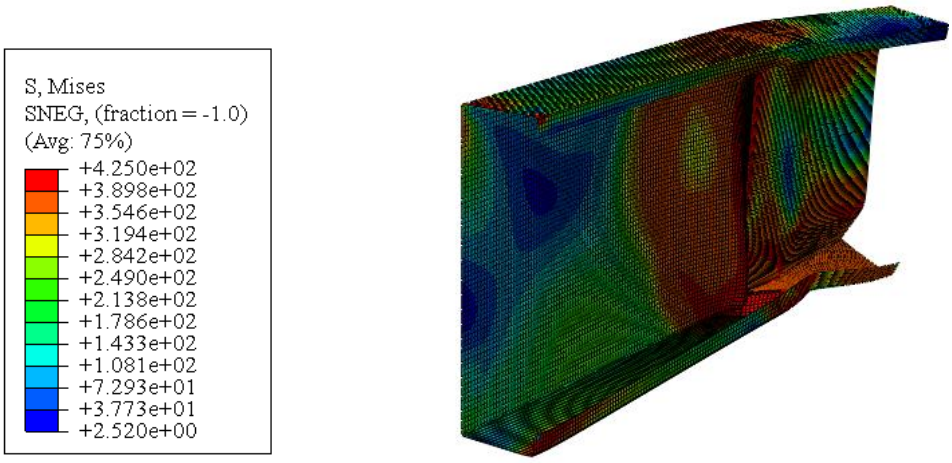

(a) FEA failure mode

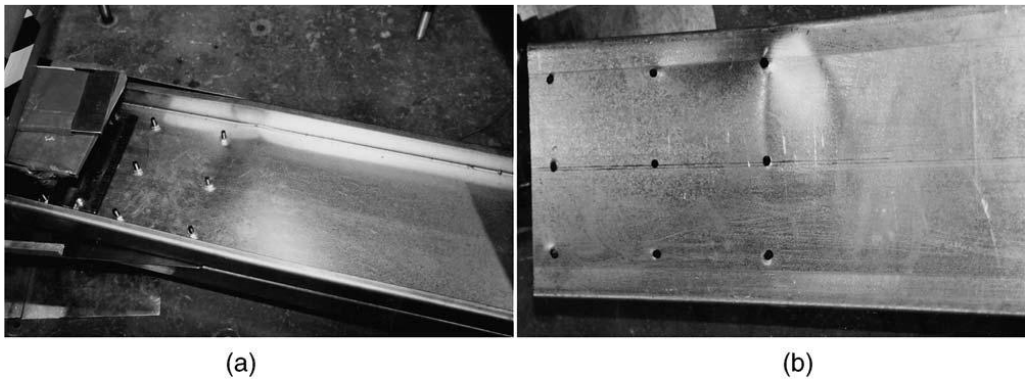

(b) Experimental Failure mode [13]

Fig. 3.7 Comparison of FEA failure mode with experimental failure mode

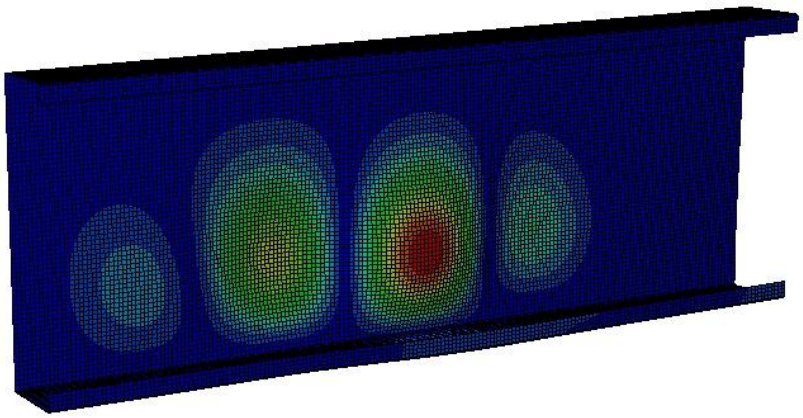

Fig. 3.8 shows buckling analysis

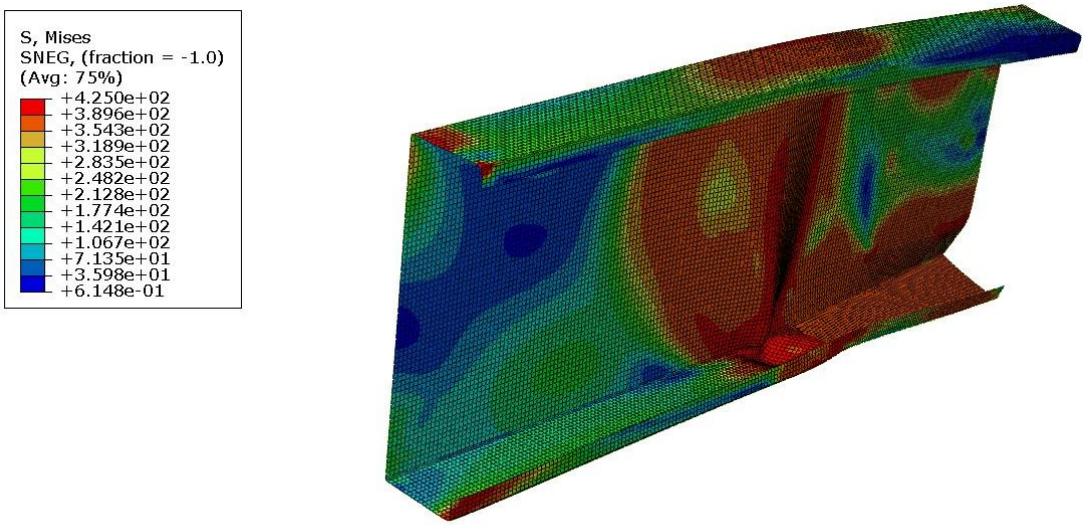

Fig. 3.9 Von Mises stress distribution showing local buckling of the web plate in the A-joint configuration.

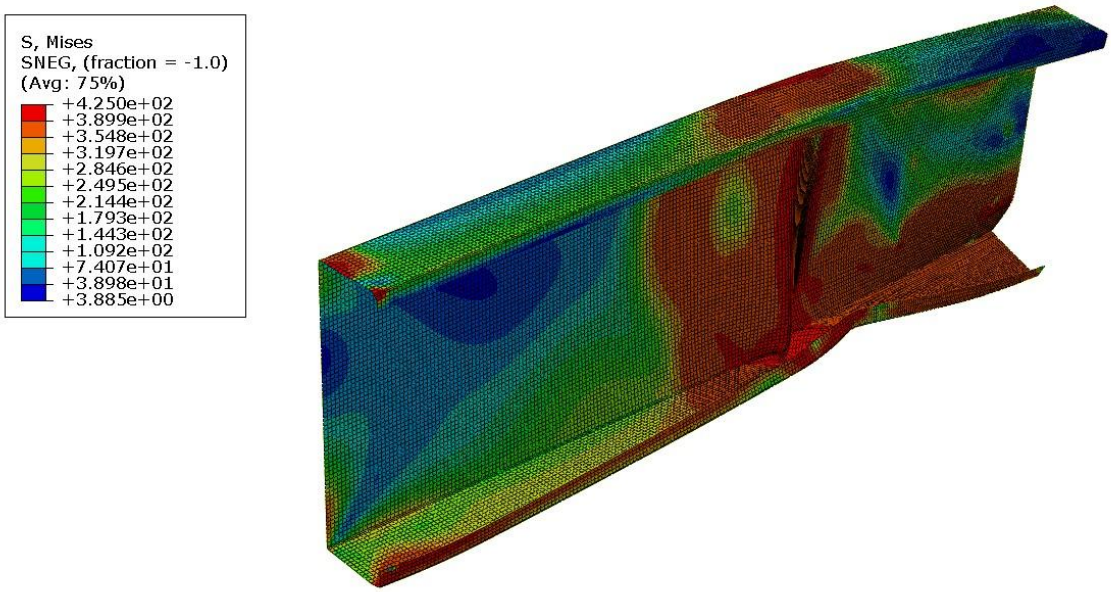

Fig. 3.10 Von Mises stress distribution showing local buckling of the web plate in the B-joint configuration.

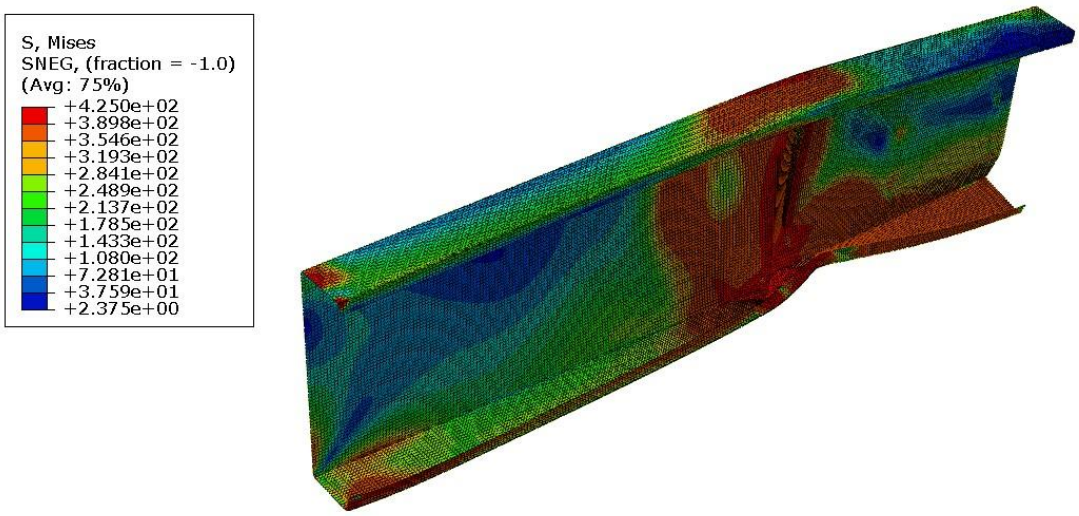

Fig. 3.11 Von Mises stress distribution showing local buckling of the web plate in the C-joint configuration.

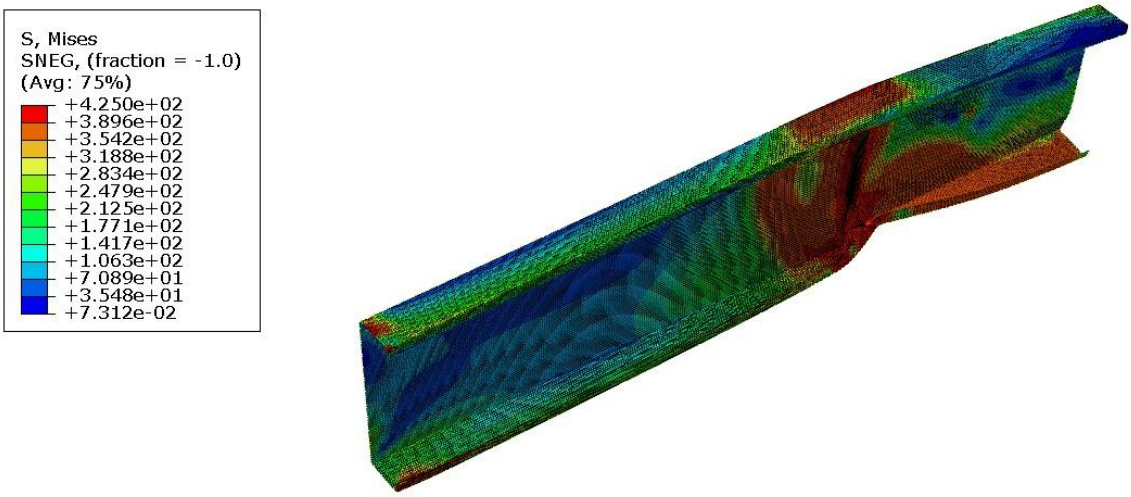

Fig. 3.12 Von Mises stress distribution showing local buckling of the web plate in the D-joint configuration.

3.10 Parametric Study

3.10.1 General

Following the validation of the FE models against experimental data, an extensive parametric study is conducted to examine the structural behaviour of CFA back-to-back channel section joints. Experimental testing is limited in its ability to cover the wide range of geometric and material variations relevant to practical applications. By contrast, FE-based parametric studies allow the controlled variation of multiple parameters and enable a deeper understanding of their influence on joint capacity. Using the validated FE model, a parametric study comprising 1008 models was conducted. This number results from the full factorial combination of the selected parameters: 6 different section depths, 4 material thicknesses, 7 a_b/d ratios, 3 bolt-group configurations, and 2 yield stresses. Multiplying these variations (6*4*7*3*2=1008) produces 1008 unique FE models. These parameters are important because each one directly affects how CFA members respond under bending. The proportions of the section influence its stiffness and its tendency to experience local or distortional buckling. Moreover, those parameters strongly influence the ultimate moment capacity.

In Table 3.4, detailed information on the parameters varied in this investigation is presented. The geometric parameters d, t and a_b/d are practical and achievable in real manufacturing. The parameter limits are chosen after reviewing the BlueScope Permalite catalogue [67], ensuring the ranges align with commercially available aluminium sections. The selected geometric ranges in Table 3.4 were systematically combined with the material properties listed in Table 3.3 to define the full matrix of FE models.

Notably, the study also incorporated H36 (5052 and 5754 series of aluminium alloys) and H38 (5052 and 5754 series of aluminium alloys) grades and tempers of aluminium alloys. These alloys are known not only for their good strength-to-weight ratio but also for their widespread use in marine, transport, and light structural applications.

Table 3-3 Summary of the material properties used in the parametric study [42]

Temper	Alloy Series of aluminium	Yield stress ($\sigma_{0.2}$)	Ultimate Stress (σ_u)	Young's Modulus (E)	ε_y	ε_u
		N/mm^2	N/mm^2	N/mm^2	%	%
H36	5052	232	272	69,400	0.54	6.10
H38	5052	250	300	68,000	0.57	7.69
H36	5754	220	290	68,000	0.52	8.41
H38	5754	270	320	68,000	0.60	7.56

Table 3-4 Selected variables in the parametric study

Channel Section	d (mm)	b_f	b_l	t	a_b/d	Bolt group	Material Properties	
							Temper	Alloy Series of Aluminium
C 150 ×25 ×10	150	25	10	[2.50-4.00]	[0.50-2.50]	2x2, 3x2 and 4x2	H-36 and H-38	5754/5052
C 200 ×30 ×15	200	30	15					
C 250 ×75 ×25	250	75	25					
C 300 ×110 ×30	300	110	30					
C 350 ×125 ×30	350	125	30					
C 400 ×125 ×30	400	125	30					

Based on the full set of numerical analyses, the results from this extensive matrix of simulations provide a comprehensive understanding of how geometric and material variations influence the moment capacity. This improved understanding enables the development of more accurate design recommendations for CFA channel section joints.

3.10.2 Effect of a_b/d

A parametric study is performed to compare the effect of a_b/d ratio on the reduced moment capacity of CFA sections. As depicted in Figs. 3.13 - 3.18, the reduced moment capacity of CFA sections with web depths of 150 mm, 200 mm, 250 mm, 300 mm, 350 mm, and 400 mm exhibits an increase with the increment in a_b/d value. For a 150 mm web depth with a 2×2 bolt group, Fig. 3.13 illustrates that the ultimate moment capacity increases from 3.77 kNm to 6.74 kNm as the a_b/d ratio increases from 0.50 to 2.50. However, it is observed that in Fig. 3.13, the moment capacity increases more than 1.5 times with the increment of a_b/d value for all the sections. The a_b/d ratio has a direct influence on the buckling behaviour of CFA channel connections. Lower a_b/d ratios show earlier buckling for 2×2, 3×2 and 4×2 bolt group, while with a higher a_b/d ratio it is found delay in buckling. In conclusion, Figs. 3.13–3.18 demonstrate that the 4×2 bolt group provides greater stability and buckling resistance compared to the 2×2 and 3×2 bolt groups.

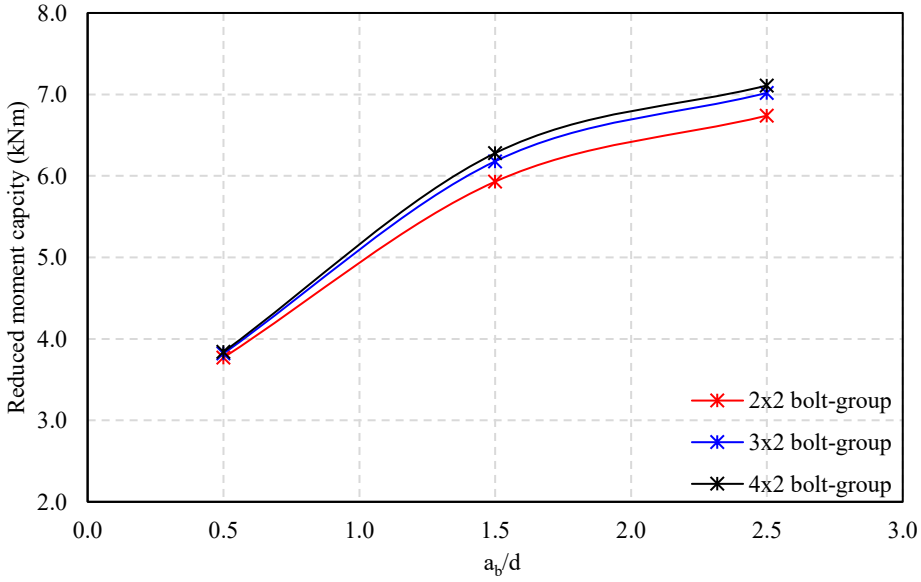

Fig. 3.13 Effect of a_b/d on reduced moment capacity showing nonlinear increase up to 7.10 kNm (web depth = 150 mm)

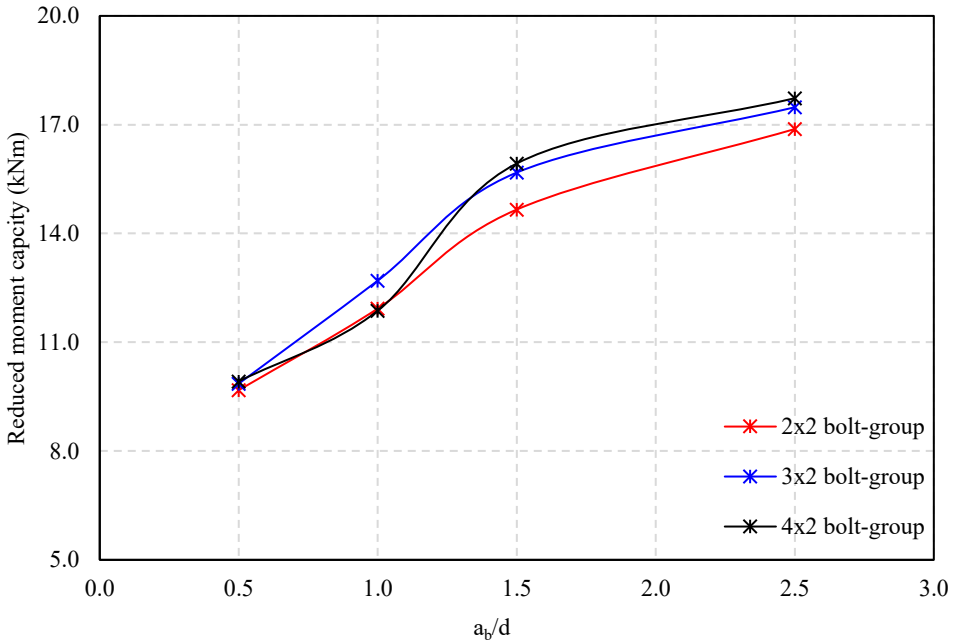

Fig. 3.14 Effect of a_b/d on reduced moment capacity showing nonlinear increase up to 17.70 kNm (web depth = 200 mm)

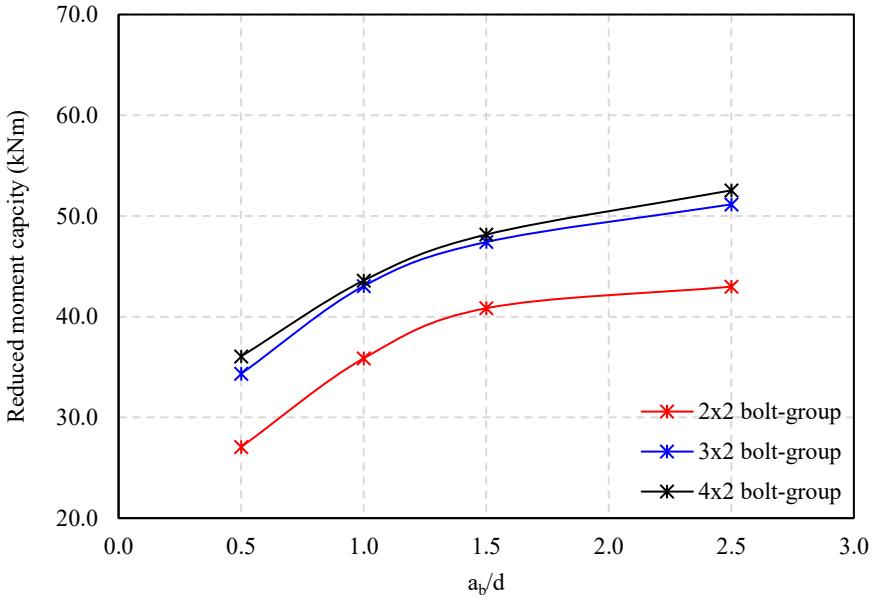

Fig. 3.15 Effect of a_b/d on reduced moment capacity showing nonlinear increase up to 52.50 kNm (web depth = 250 mm)

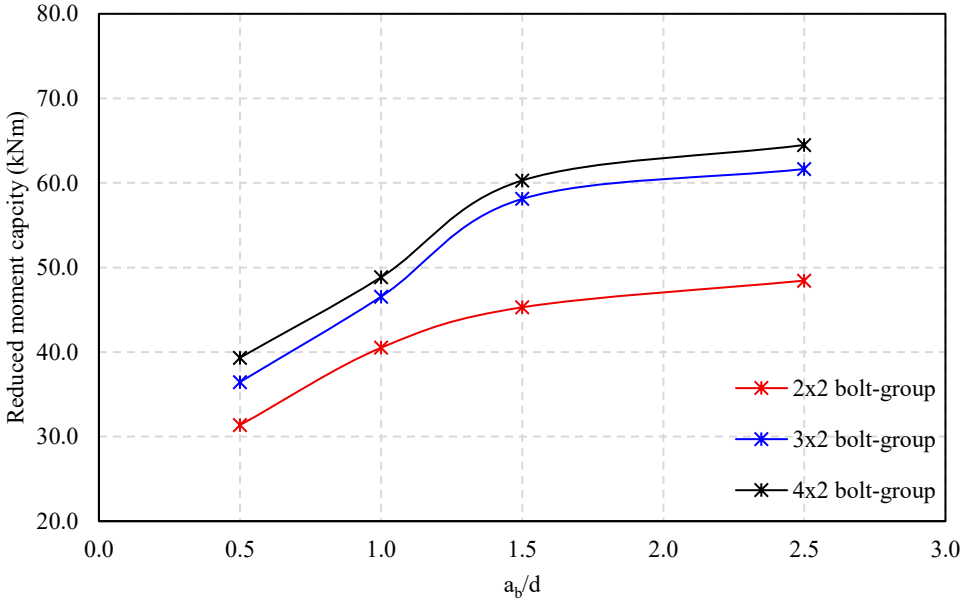

Fig. 3.16 Effect of a_b/d on reduced moment capacity showing nonlinear increase up to 64.50 kNm (web depth = 300 mm)

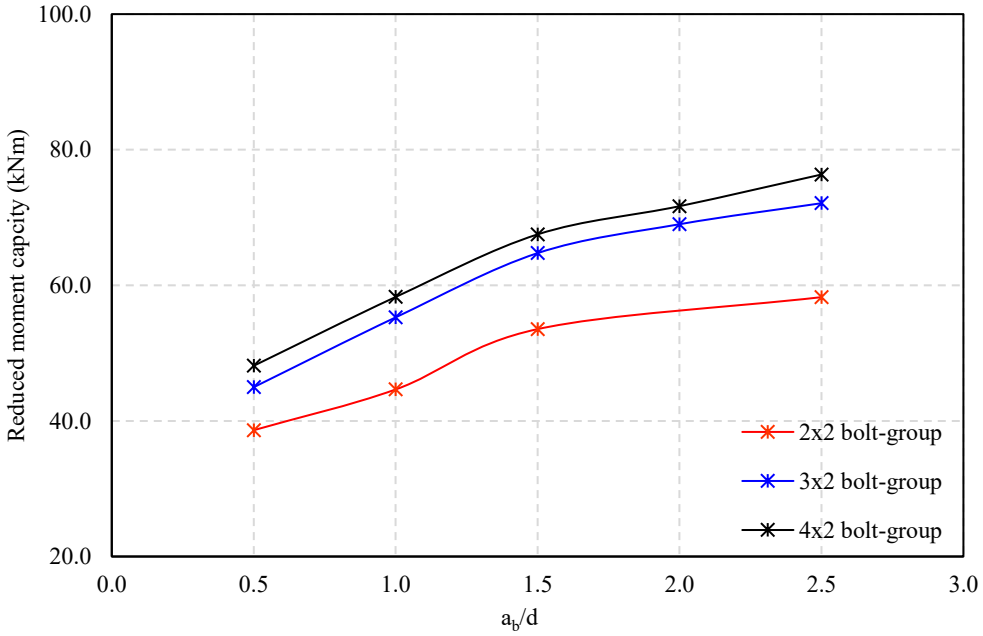

Fig. 3.17 Effect of a_b/d on reduced moment capacity showing nonlinear increase up to 76.30 kNm (web depth = 350 mm)

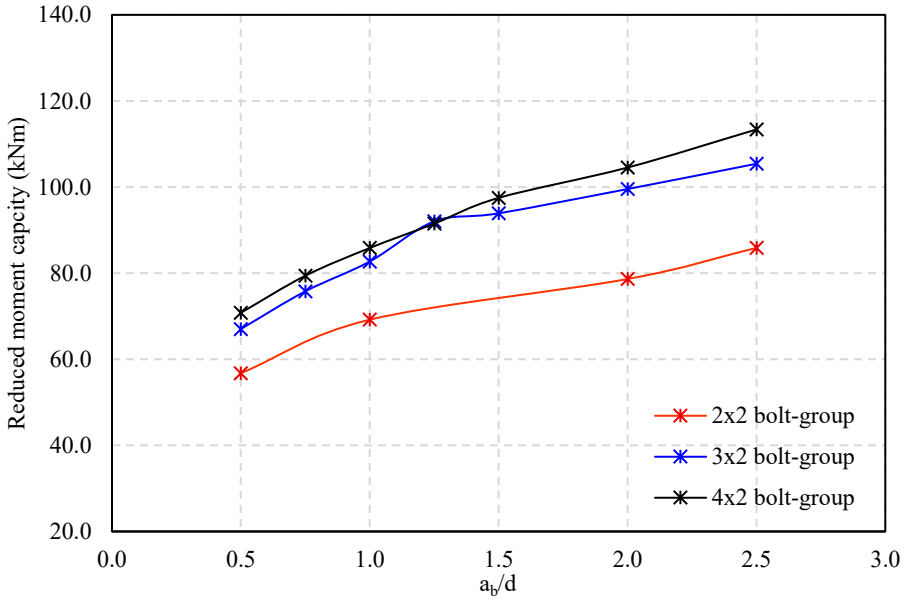

Fig. 3.18 Effect of a_b/d on reduced moment capacity showing nonlinear increase up to 113.40 kNm (web depth = 400 mm)

3.10.3 Effect of d/t

The parametric study further investigates the effect of d/t ratio on reduced moment capacity of CFA sections. Figs. 3.19 - 3.24 illustrates the effect of d/t ratio on the reduced moment capacity of CFA sections. A downward trend is observed in Figs. 3.19 - 3.24. While the d/t value is increasing, the ultimate moment capacity is gradually reducing for the 2×2, 3×2 and 4×2 bolt group and bolt group 2×2 has lower moment capacity than bolt group 3×2 and bolt group 4×2. For the bolt group 4×2, increasing the slenderness ratio d/t from 100 to 160 the ultimate moment capacity is found from 93.00 kNm to 39.66 kNm, representing a 57% reduction. Ultimate moment capacity decreases by about 57 % and 55% for bolt group 3×2 and 2×2 also. The normalized capacity decreased from 1.0 to 0.43 and 0.45 for those bolt group. Figs. 3.19 - 3.24 shows a clear inverse relationship between the d/t ratio and moment capacity of CFA channel connections. As sections become more slender, local buckling occurs earlier and leading to significant reductions in reduced moment capacity. At low d/t ratios, it provides

greater stiffness, delaying buckling and ensuring higher ultimate moment capacity. The number and arrangement of bolts also play an important role in how the section behaves against buckling. However, after analyzing figs. 3.19 - 3.24, it is shown that at higher slender sections, even larger bolt groups cannot completely prevent buckling. In summary, larger bolt groups contribute to delaying buckling and enhancing reduced moment capacity across different types of channel sections.

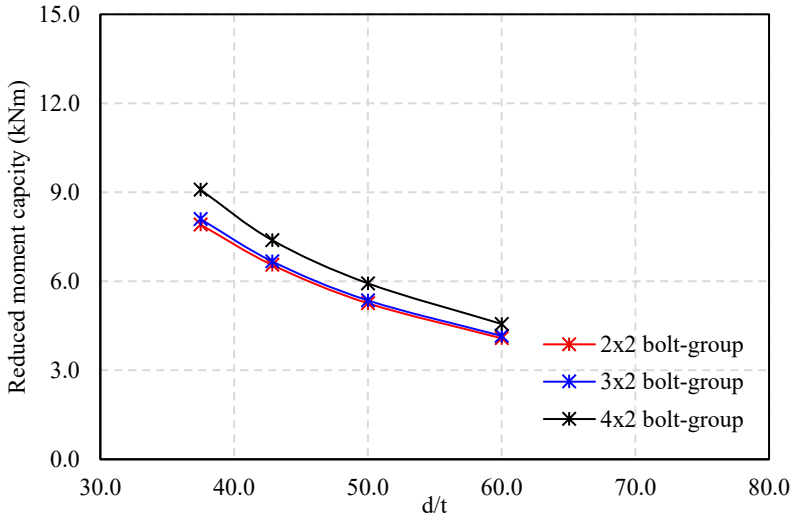

Fig. 3.19 Effect of d/t on reduced moment capacity showing nonlinear decline up to 4.20 kNm (web depth = 150 mm)

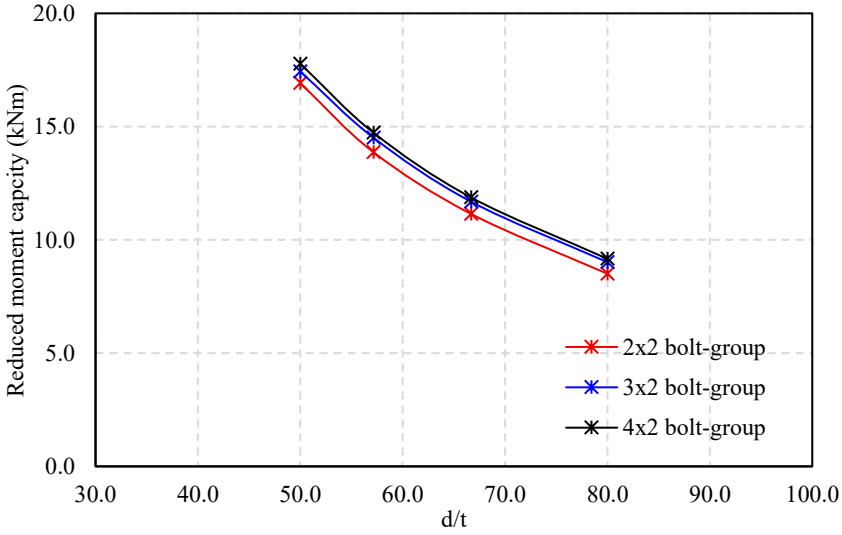

Fig. 3.20 Effect of d/t on reduced moment capacity showing nonlinear decline up to 8.50 kNm (web depth = 200 mm)

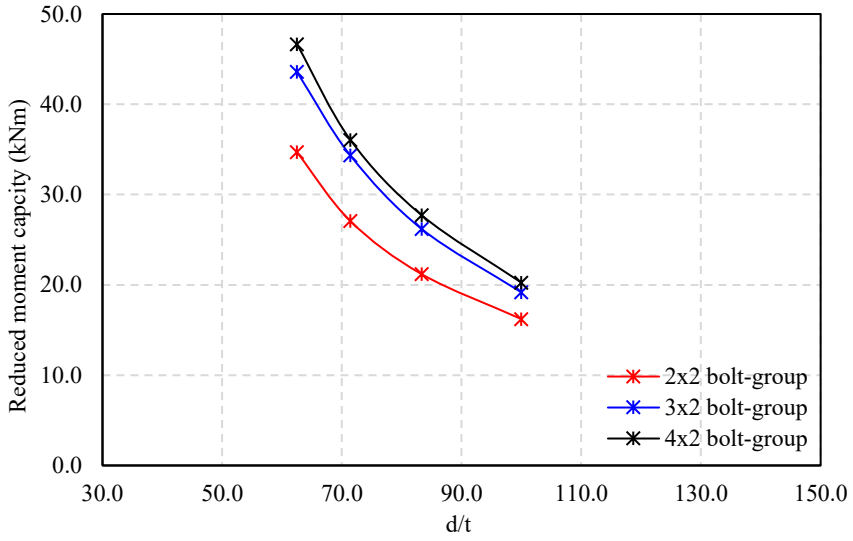

Fig. 3.21 Effect of d/t on reduced moment capacity showing nonlinear decline up to 16.20 kNm (web depth = 250 mm)

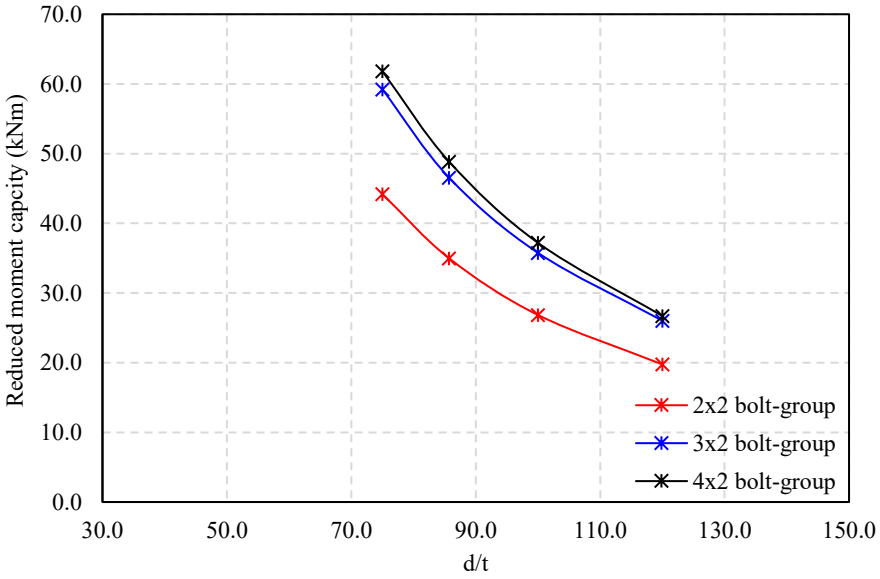

Fig. 3.22 Effect of d/t on reduced moment capacity showing nonlinear decline up to 19.70 kNm (web depth = 300 mm)

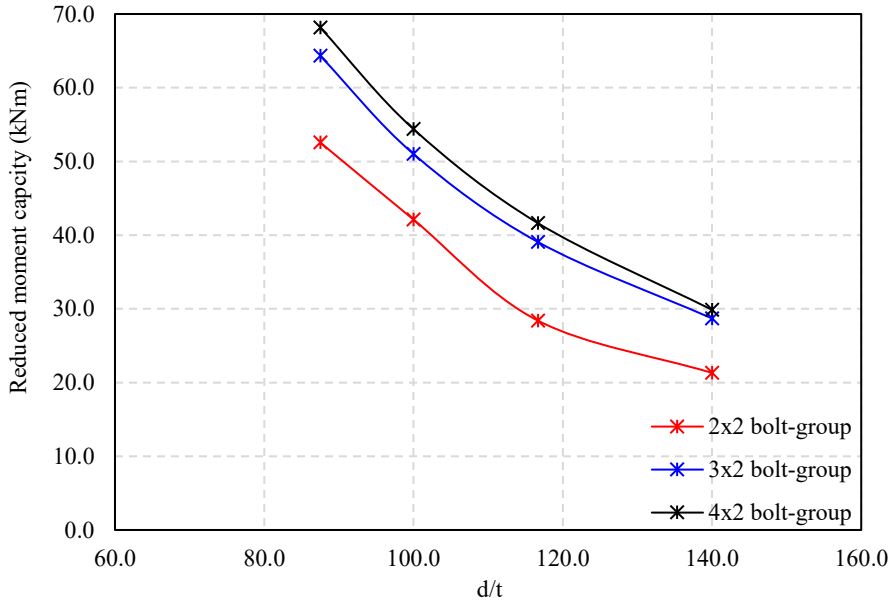

Fig. 3.23 Effect of d/t on reduced moment capacity showing nonlinear decline up to 21.30 kNm (web depth = 350 mm)

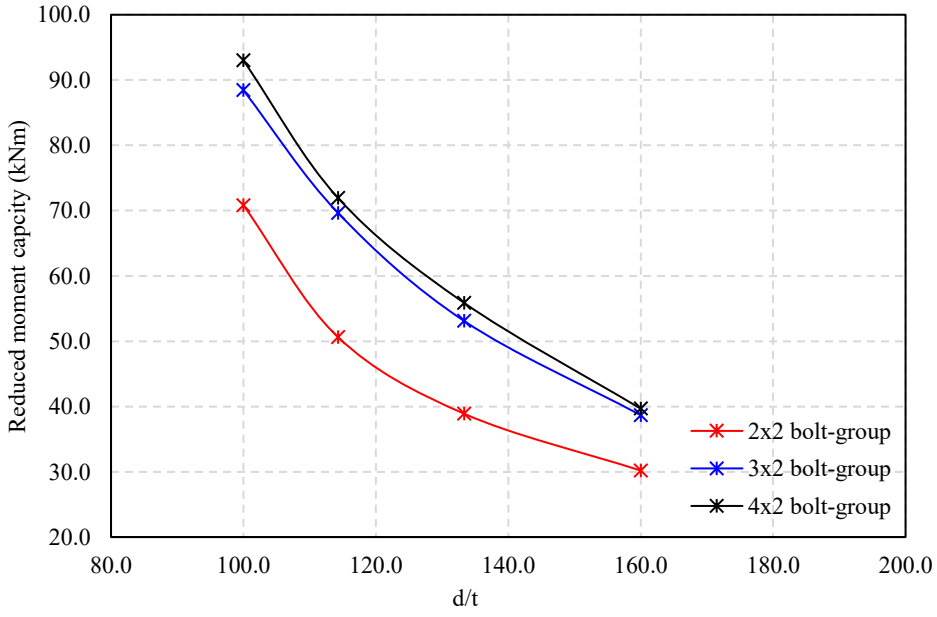

Fig. 3.24 Effect of d/t on reduced moment capacity showing nonlinear decline up to 30.20 kNm (web depth = 400 mm)

3.10.4 Effect of b_d/t on reduced moment capacity

The study also examines the effect of b_d/t on the reduced moment capacity. Here, b_d represents the bolt group spacing, which is calculated using the formula $b_d = a_b/N$, where N is the number of spacings between the bolt groups. As shown in Figs. 3.25 - 3.30, the reduced moment capacity of CFA sections with web depths of 150 mm, 200 mm, 250 mm, 300 mm, 350 mm, and 400 mm demonstrates a downward trend with the increment in bolt group spacing. When the b_d/t ratio increases, the ultimate moment capacity reaches minimum as local buckling governs earlier. But a lower b_d/t ratio enhances stability and increases the ultimate moment capacity. Compared to larger bolt groups, the 2×2 bolt group has fewer bolts and less confinement. This makes the connection more slender and more prone to local buckling. Moreover, at higher value of b_d/t, the moment capacity of 2×2 bolt group is lower than other bolt groups. This trend is observed in Figs. 3.25 - 3.30 with the increase in web depth from 150 mm to 400 mm. Additionally, Figs. 3.25 - 3.30 indicate that the ultimate moment capacity is highest at a web depth of 400 mm and lowest at 150 mm. This confirms that smaller bolt groups provide less stability against buckling. Furthermore, for a web depth of 150 mm, the average difference in ultimate moment capacity among the 2×2, 3×2, and 4×2 bolt groups is 1.55%. This difference increases progressively with web depth, reaching 6.56% at 200 mm, 20.55% at 250 mm, 27.50% at 350 mm, and 29.12% at 400 mm, although a lower value of 18.86% is observed at 300 mm. It can be concluded that the influence of bolt group spacing on ultimate moment capacity becomes increasingly significant with greater web depth, and adding more bolts leads to the highest ultimate moment capacity for CFA channel sections.

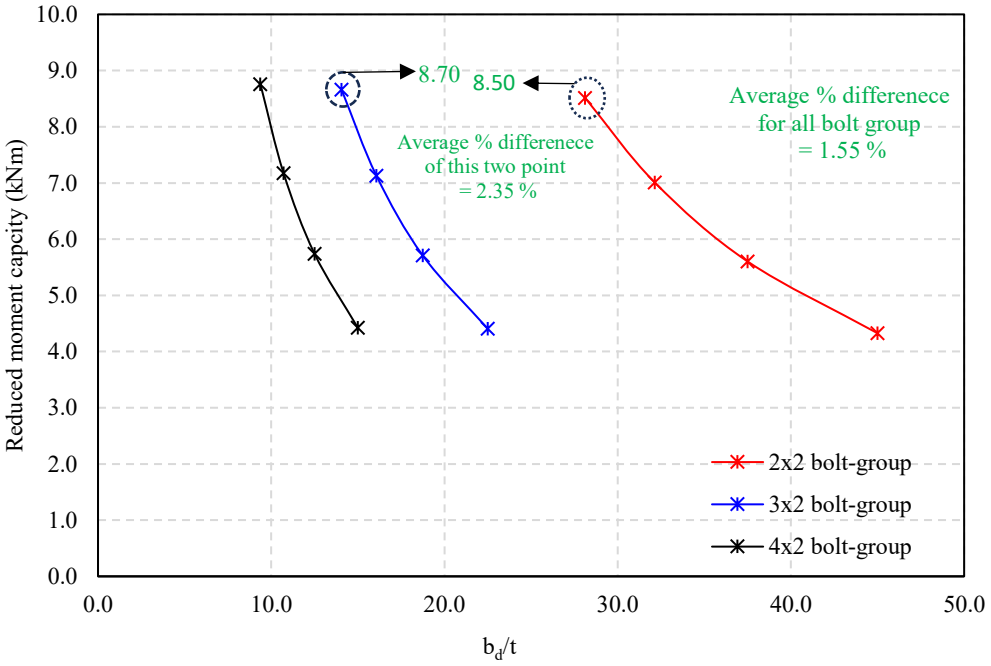

Fig. 3.25 Effect of b_d/t on reduced moment capacity demonstrating nonlinear reduction up to 4.30 kNm (web depth = 150 mm)

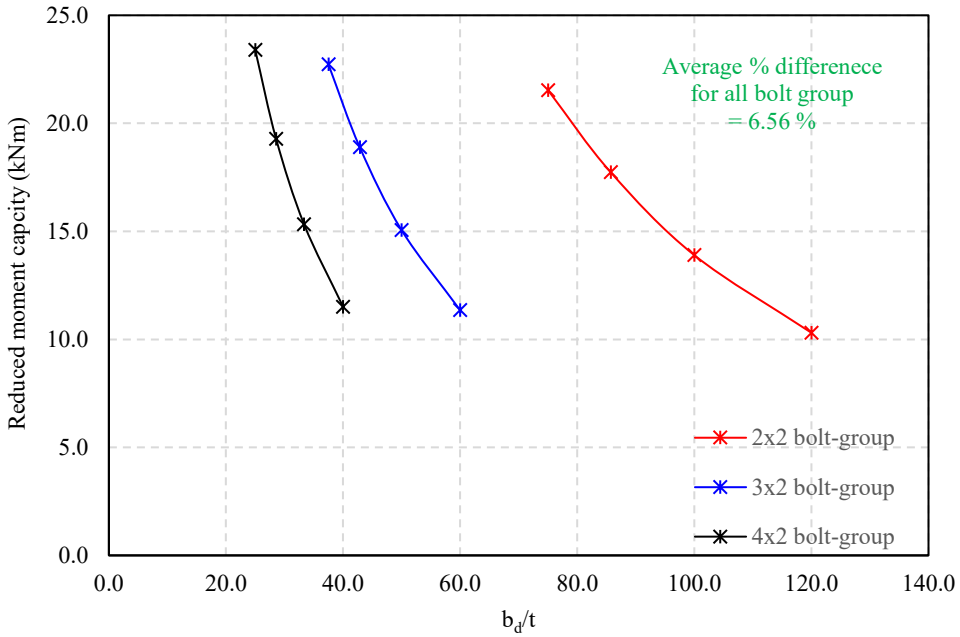

Fig. 3.26 Effect of b_d/t on reduced moment capacity demonstrating nonlinear reduction up to 10.30 kNm (web depth = 200 mm)

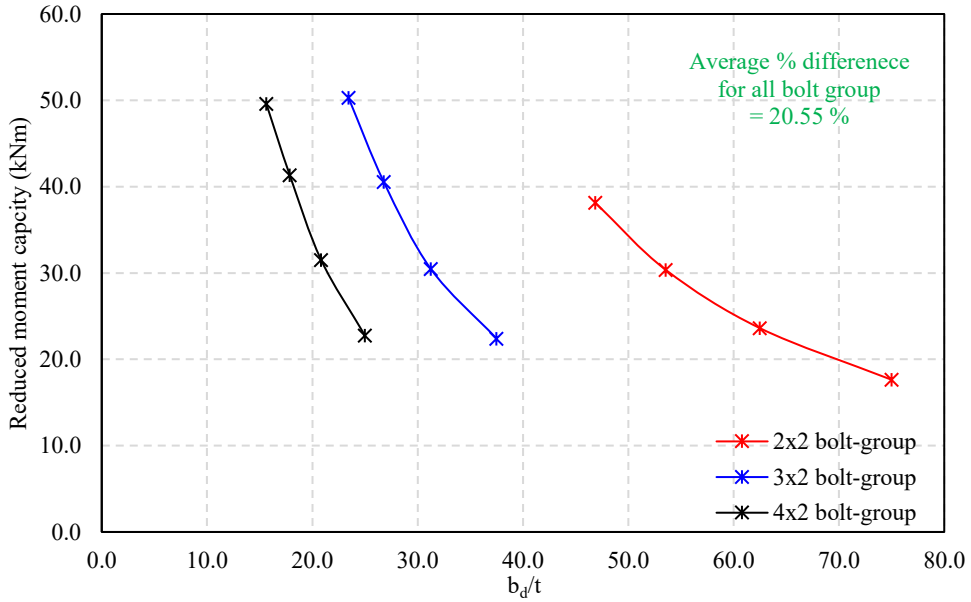

Fig. 3.27 Effect of b_d/t on reduced moment capacity demonstrating nonlinear reduction up to 17.60 kNm (web depth = 250 mm)

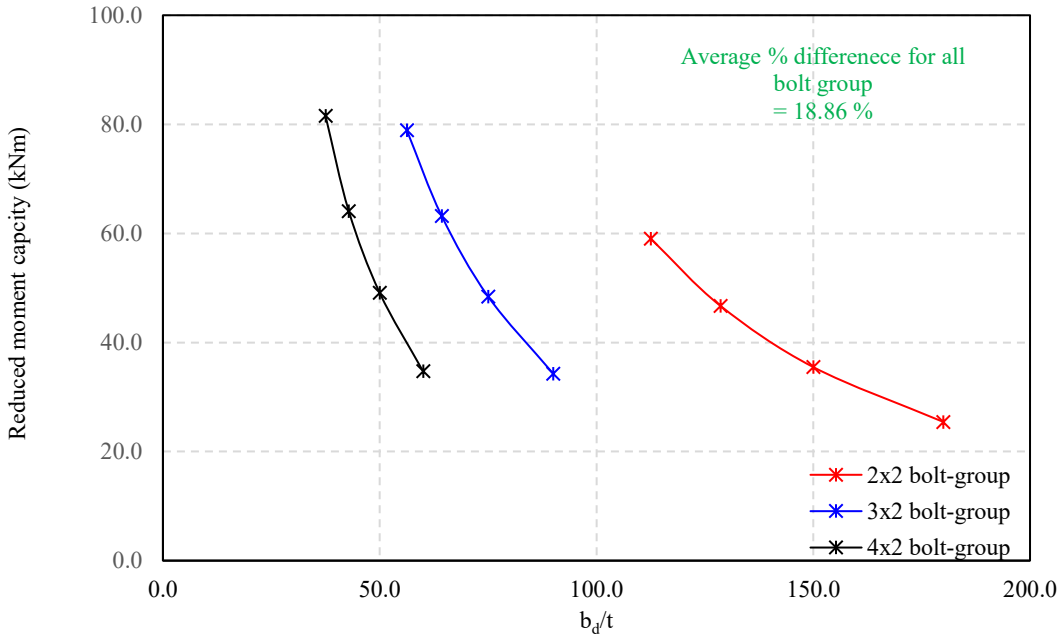

Fig. 3.28 Effect of b_d/t on reduced moment capacity demonstrating nonlinear reduction up to 25.40 kNm (web depth = 300 mm)

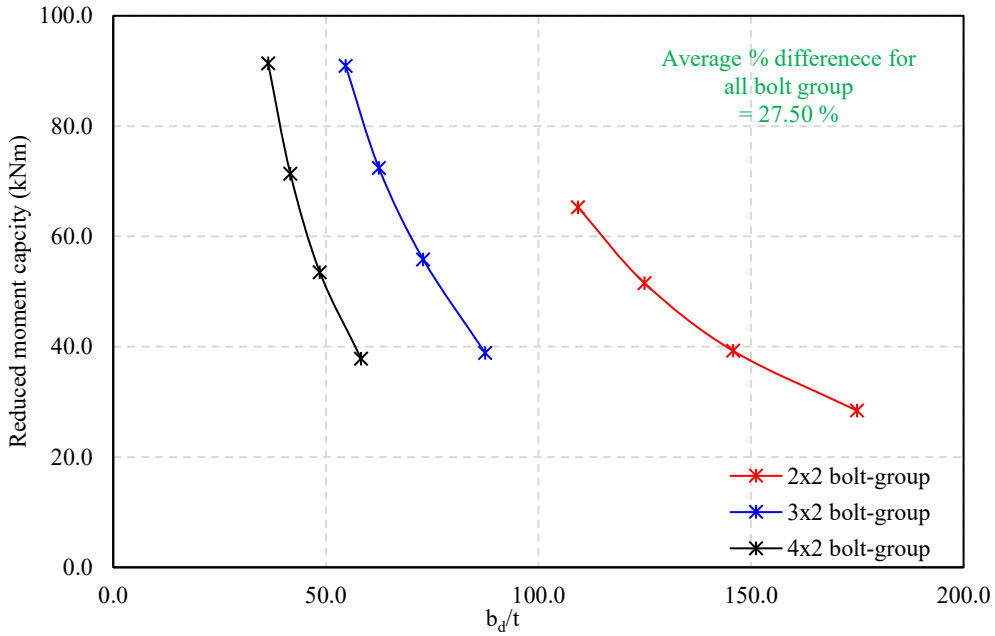

Fig. 3.29 Effect of b_d/t on reduced moment capacity demonstrating nonlinear reduction up to 28.40 kNm (web depth = 350 mm)

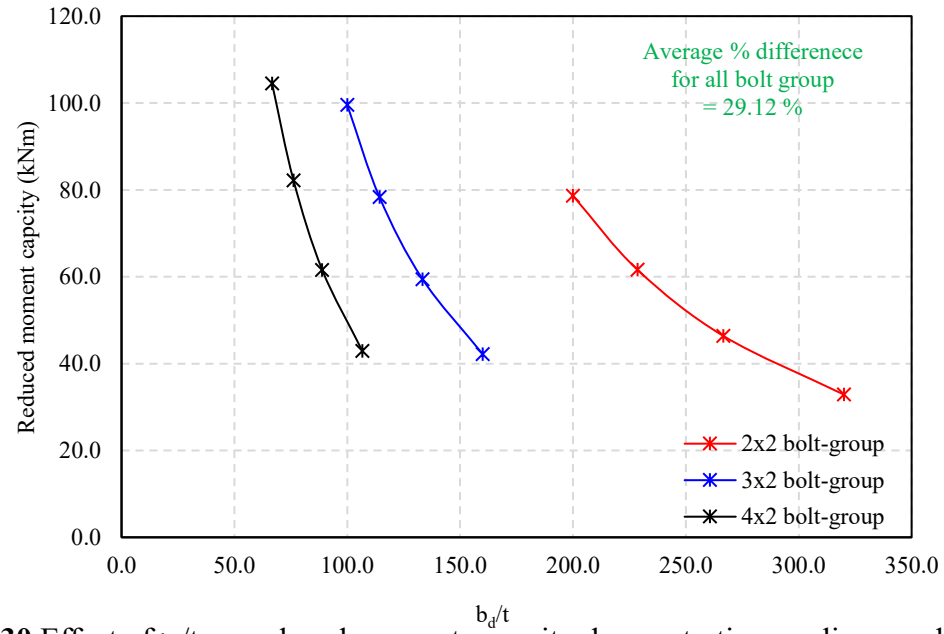

Fig. 3.30 Effect of b_d/t on reduced moment capacity demonstrating nonlinear reduction up to 32.90 kNm (web depth = 400 mm)

3.10.5 Interaction between d/t and a_b/d

The ratio d/t represents how slender the section is, while a_b/d describes how far apart the bolts are relative to the section depth. When d/t increases, the plates become thinner and less stiff, making them more likely to buckle early. Increasing a_b/d can provide more rotational restraint and improve joint performance, but this effect becomes much smaller in very slender sections. In those cases, local buckling of the thin plates occurs first, so increasing bolt spacing cannot prevent the loss of capacity. Overall, the interaction between d/t and a_b/d indicates that section slenderness governs joint behaviour, and increases in bolt spacing provide limited benefit once buckling becomes the dominant failure mode.

3.10.6 Interaction between d/t and b_d/t

The ratio d/t describes the overall slenderness of the section, while b_d/t represents the relative spacing of the bolt groups compared to thickness, where $b_d = a_b/N$. As d/t increases, the section becomes more slender and less stiff, making it more susceptible to buckling. Increasing b_d/t means the bolt groups are spaced further, which reduces local restraint and increases the tendency for local buckling. When both d/t and b_d/t are high, buckling occurs earlier and governs the joint behaviour, whereas lower values of these ratios result in stiffer joints with higher resistance. Finally, the interaction between d/t and b_d/t shows that increasing section slenderness and bolt group spacing together accelerates buckling.

3.10.7 Relationship between failure mode transitions and d/t, a_b/d and bolt group configuration

As d/t increases, the section becomes more slender and less stiff. At low d/t, the section remains stable and buckling is delayed, allowing distortional effects to develop. At higher d/t, local plate buckling occurs earlier and dominates the failure mode. Additionally, smaller a_b/d values result in closely spaced bolts, increasing joint restraint and favouring distortional buckling of the section. As a_b/d increases, the

restraint becomes weaker, which shifts the failure mode toward local buckling. In addition, bolt group configuration influences how forces are distributed and how much restraint the joint provides. Configurations with more bolt rows or tighter spacing offer greater restraint and promote distortional or mixed buckling modes. In contrast, configurations with fewer bolts or wider spacing reduce restraint and allow local buckling to develop earlier. As a result, changes in bolt group configuration can shift the failure mode between distortional, mixed, and local buckling.

Table 3-5 shows failure mode of all channel sections

Channel Section	d (mm)	b_f	b_l	t	a_b/d	Mode of Failure
C 150 ×25 ×10	150	25	10	[2.50-4.00]	[0.50-2.50]	Local buckling
C 200 ×30 ×15	200	30	15			Local buckling
C 250 ×75 ×25	250	75	25			Local buckling
C 300 ×110 ×30	300	110	30			Local buckling
C 350 ×125 ×30	350	125	30			Local buckling
C 400 ×125 ×30	400	125	30			Local buckling

Chapter 4- Comparison with Direct Strength Method guidelines

4.1 Introduction

In this chapter, the FEA results are compared with the predictions obtained from the Direct Strength Method (DSM). The comparison allows us to see how closely the guideline-based method aligns with the numerical findings, and whether DSM tends to be conservative or unconservative for CFA sections. This step is important because it helps to assess whether existing design provisions are suitable for aluminium or if adjustments are needed to capture their behaviour more accurately. Furthermore, the FEA results are also compared with the findings of Lim and Nethercot [13] and Mojtabaei et al. [12]. Based on this comparison, a modification to the equation proposed by Lim and Nethercot [13] is developed. This modification aims to enhance the predictive accuracy and establish a more robust design framework for aluminium structural components.

4.2 Comparison between DSM and FEA for reduced moment capacity

The introduction of the Direct Strength Method (DSM) provides a design approach specifically suited to cold-formed steel members, allowing moment capacity to be calculated directly by accounting for local, distortional, and global buckling, without the need for effective width calculations (Schafer & Peköz,) [63]. In this study, the reduced moment capacities obtained from the DSM [64, 65] are compared with FEA for CFA. Based on the comparison of 1008 data points, the DSM predictions overestimated the FEA-derived moment capacities by an average of approximately 30.30%. The moment capacities predicted by FEA are lower than those obtained from DSM. This is mainly due to bolt group effects, shear lag, and the interaction between shear and bending.

DSM assumes the connections at the member ends are perfectly rigid, meaning the entire section is expected to carry bending moments uniformly. However, bolted joints are flexible because of small slips, bolt-hole elongation, and uneven stress around the bolts in practice. FEA captures these effects by including contact behaviour and bolt deformation, showing that some bolts carry higher stresses while others carry less. This flexibility reduces the joint stiffness and lowers the overall moment capacity. Schafer & Peköz [63] noted that ignoring this local yielding and deformation can lead to unrealistically uniform stress assumptions. Therefore, DSM tends to overestimate the strength because it does not include this connection flexibility. In an ideal case, DSM assumes that every part of the flange carries the same amount of bending stress. However, in reality, the parts of the flange closer to the web carry higher stress, while the outer edges of the flange carry less stress. This happens because the shear flow between the web and flange does not spread uniformly. As a result, not all of the flange area contributes fully to resisting bending. Therefore, DSM overestimates strength because it assumes the entire flange is equally effective in bending. In thin-walled channel sections, the shear stresses in the web combine with bending stresses, especially near bolt groups and loading points. DSM considers shear and bending separately, but in reality, they act together. FEA captures this combined behaviour, showing that shear strain can cause early yielding and local buckling in the web. This interaction reduces stiffness and results in lower ultimate moment capacity in FEA compared to the higher values predicted by DSM.

Overall, DSM overestimates the moment capacity of cold-formed aluminium joints because it does not capture connection flexibility, shear lag, and shear bending interaction.

For local buckling:

$$M_{b\ell} = M_y \text{ for } \lambda_\ell \leq 0.776 \tag{4.1}$$

$$M_{b\ell} = \left[1 - 0.15\left(\frac{M_{o\ell}}{M_y}\right)^{0.4}\right]\left(\frac{M_{o\ell}}{M_y}\right)^{0.4} M_y \text{ for } \lambda_\ell > 0.776 \tag{4.2}$$

$$\lambda_\ell = \sqrt{\frac{M_y}{M_{o\ell}}} \tag{4.3}$$

For distortional buckling:

$$M_{bd} = M_y \text{ for } \lambda_d \leq 0.561 \tag{4.4}$$

$$M_{bd} = \left[1 - 0.25\left(\frac{M_{od}}{M_y}\right)^{0.6}\right]\left(\frac{M_{od}}{M_y}\right)^{0.6} M_y \text{ for } \lambda_d > 0.561 \tag{4.5}$$

$$\lambda_d = \sqrt{\frac{M_y}{M_{od}}} \tag{4.6}$$

In this study, using the following equations (Eqs 4.1- 4.6). the ultimate moment capacity for DSM is found and used the minimum value for this paper. As the initial value for FEA is determined for a single channel section, the minimum value is determined twice. Figs. 4.1 - 4.18 illustrate the comparison of FEA and DSM on CFA sections for different bolt group.

For bolt group 2×2:

The comparison between DSM and FEA results for a web depth of 150 mm yielded an R^2 value of 0.49, a mean bias of 1.54, and a coefficient of variation of 0.22. These results indicate that DSM predictions exhibit only a moderate correlation with the FEA data and generally overestimate the reduced moment capacities by approximately 54%. For a web depth of 200 mm, the analysis produced an R^2 value of 0.72, a mean bias of 1.18, and a coefficient of variation of 0.16. These findings suggest a reasonably good correlation between the two methods, with DSM overestimating the reduced moment capacities by around 18%.

For a web depth of 250 mm, the comparison yielded an R^2 value of 0.78, a mean bias of 1.60, and a coefficient of variation of 0.26. These results demonstrate a good correlation between DSM and FEA moment capacities, though DSM tends to overpredict the strength by approximately 60%. Similarly, for a web depth of 300 mm, a good correlation was also observed, with an R^2 value of 0.75, a mean bias of 1.95, and a coefficient of variation of 0.28. But the value of mean bias indicates that DSM overestimates the FEA strength by about 95%.

For a web depth of 350 mm, an R^2 value of 0.77, a mean bias of 1.72, and a coefficient of variation of 0.24 were obtained, indicating better agreement between FEA and DSM predictions. On the other hand, DSM tends to overpredict the strength by approximately 72%. Finally, for a web depth of 400 mm, the R^2 value was 0.80, the mean bias 1.58, and the coefficient of variation 0.21, which confirms strong correlation and DSM overpredicts the strength by approximately 58%.

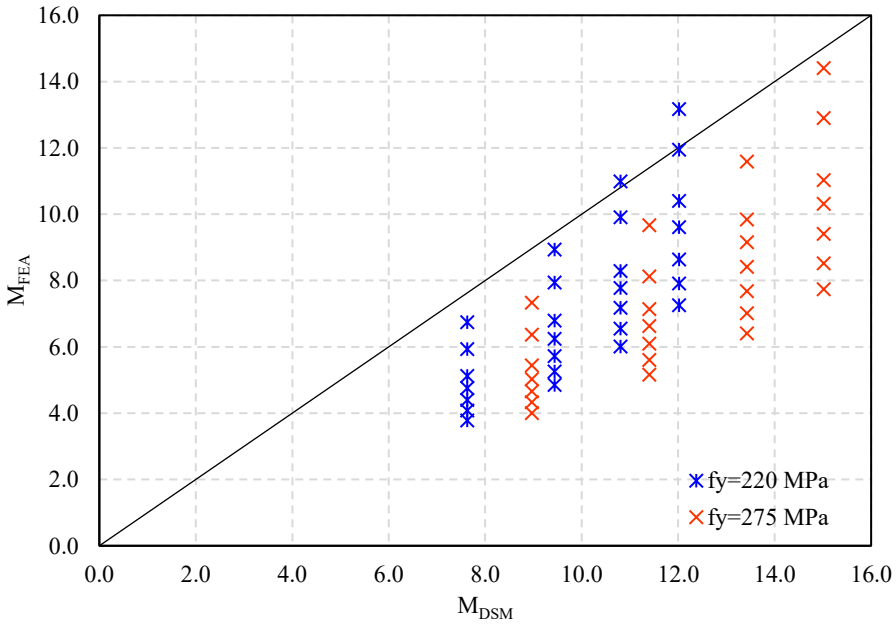

Fig. 4.1 Comparison of reduced moment capacity between DSM and FEA (web depth = 150 mm)

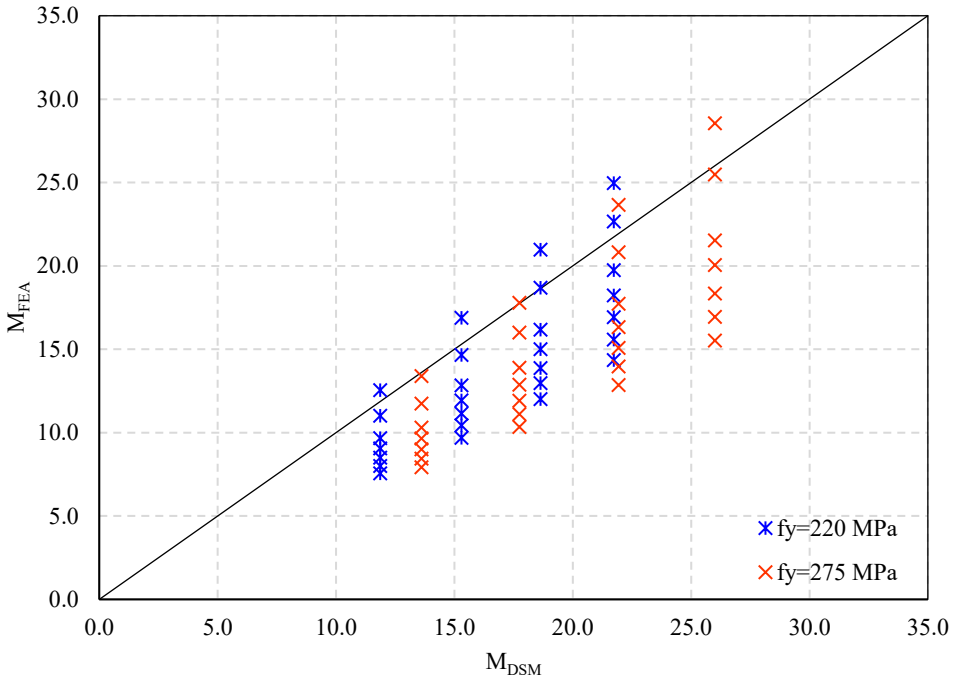

Fig. 4.2 Comparison of reduced moment capacity between DSM and FEA (web depth = 200 mm)

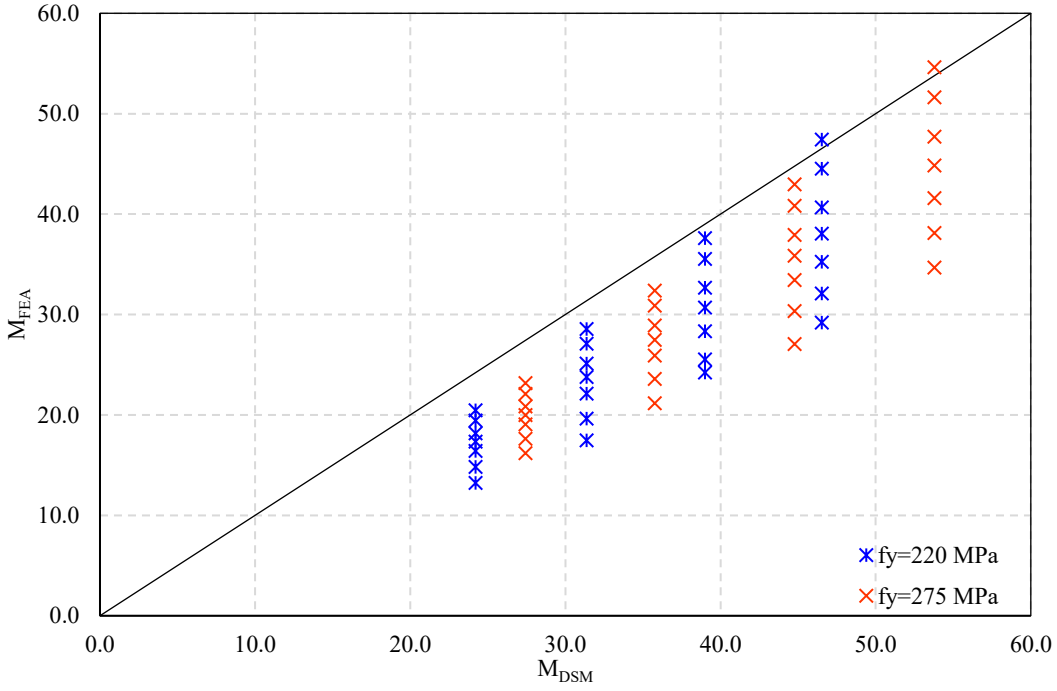

Fig. 4.3 Comparison of reduced moment capacity between DSM and FEA (web depth = 250 mm)

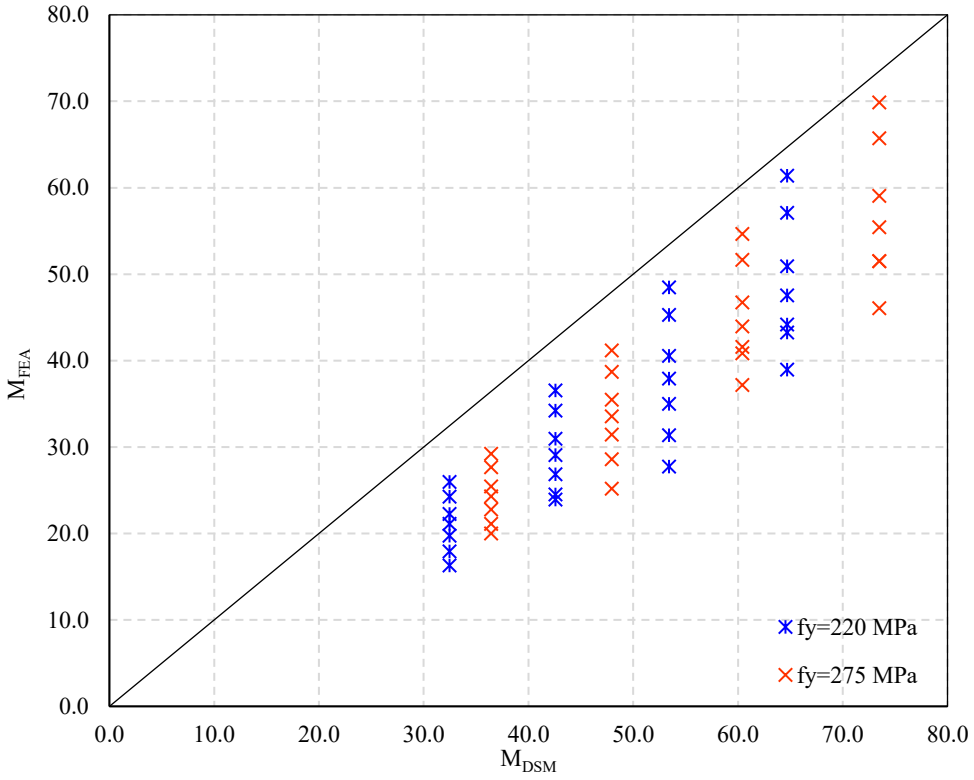

Fig. 4.4 Comparison of reduced moment capacity between DSM and FEA (web depth = 300 mm)

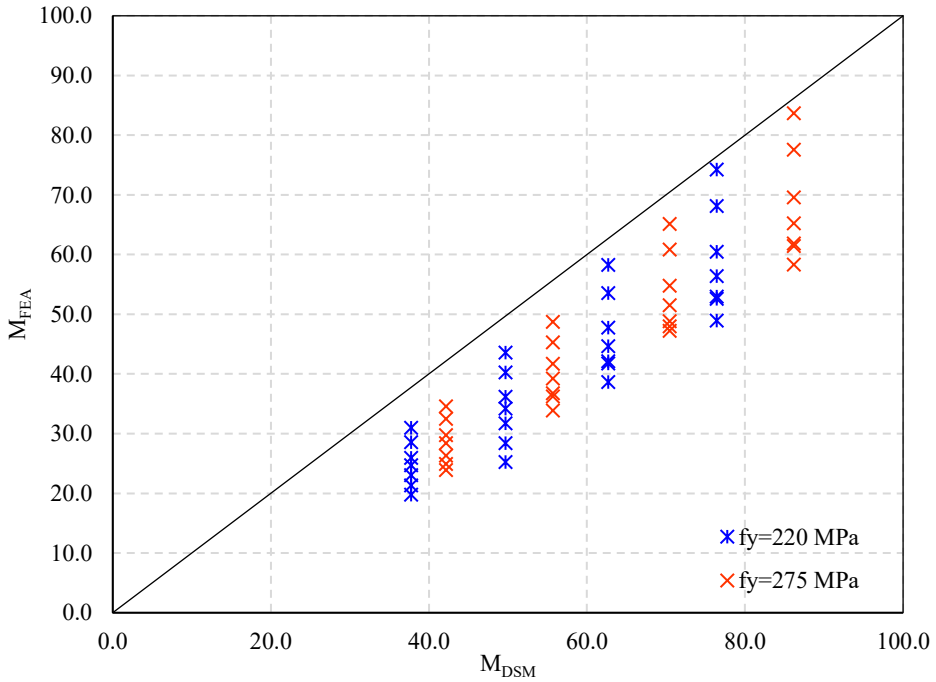

Fig. 4.5 Comparison of reduced moment capacity between DSM and FEA (web depth = 350 mm)

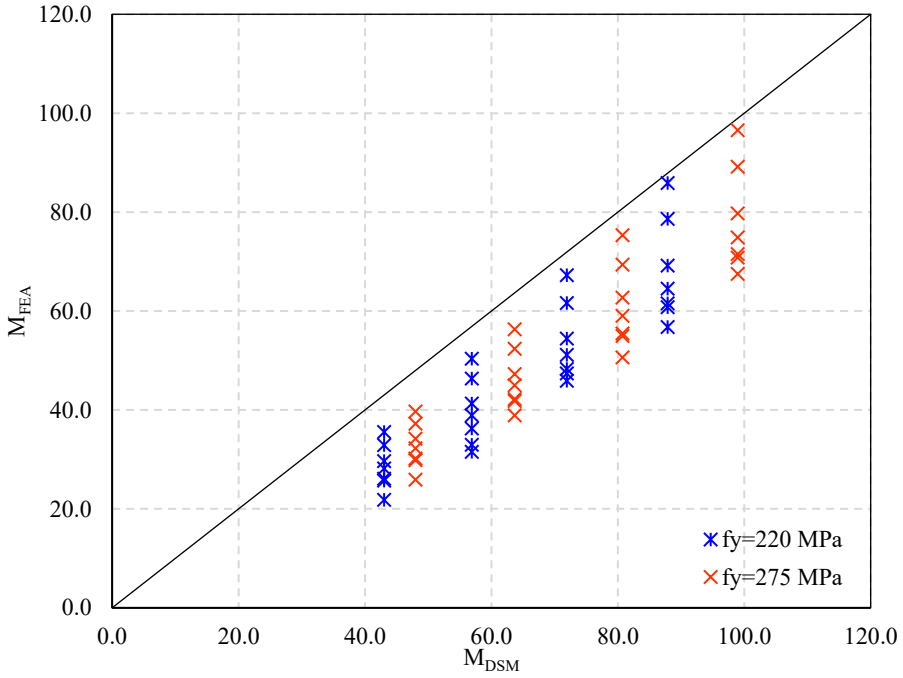

Fig. 4.6 Comparison of reduced moment capacity between DSM and FEA (web depth = 400 mm)

For bolt group 3×2:

The comparison between DSM and FEA results for a web depth of 150 mm yielded an R^2 value of 0.51, a mean bias of 1.62, and a coefficient of variation of 0.23. These results indicate that DSM predictions exhibit only a moderate correlation with the FEA data and generally overestimate the reduced moment capacities by approximately 62%. For a web depth of 200 mm, the analysis produced an R^2 value of 0.73, a mean bias of 1.20, and a coefficient of variation of 0.17. These findings suggest a strong correlation between the two methods, with DSM overestimating the reduced moment capacities by around 20%.

The comparison for a web depth of 250 mm yielded an R^2 value of 0.69, a mean bias of 1.46, and a coefficient of variation of 0.21. These results demonstrate a good correlation between the DSM and FEA moment capacities, with DSM tending to overpredict the strength by approximately 46%.

Similarly, for a web depth of 300 mm, the correlation between FEA and DSM predictions remains strong, with an average bias of 1.63, an R^2 value of 0.74, and a coefficient of variation of 0.25. But the mean bias indicates that DSM overestimates the FEA strength by about 63%.

For a web depth of 350 mm, an R^2 value of 0.76, a mean bias of 1.44, and a coefficient of variation of 0.19 were obtained, indicating a high degree of consistency between the FEA and DSM predictions. Nevertheless, DSM overpredicts the reduced moment capacity by 44%. Finally, for a web depth of 400 mm, the R^2 value was 0.78, the mean bias 1.36, and the coefficient of variation 0.18. Here, DSM overpredict the reduced moment capacity by 36% but the correlation between FEA and DSM predictions remains good.

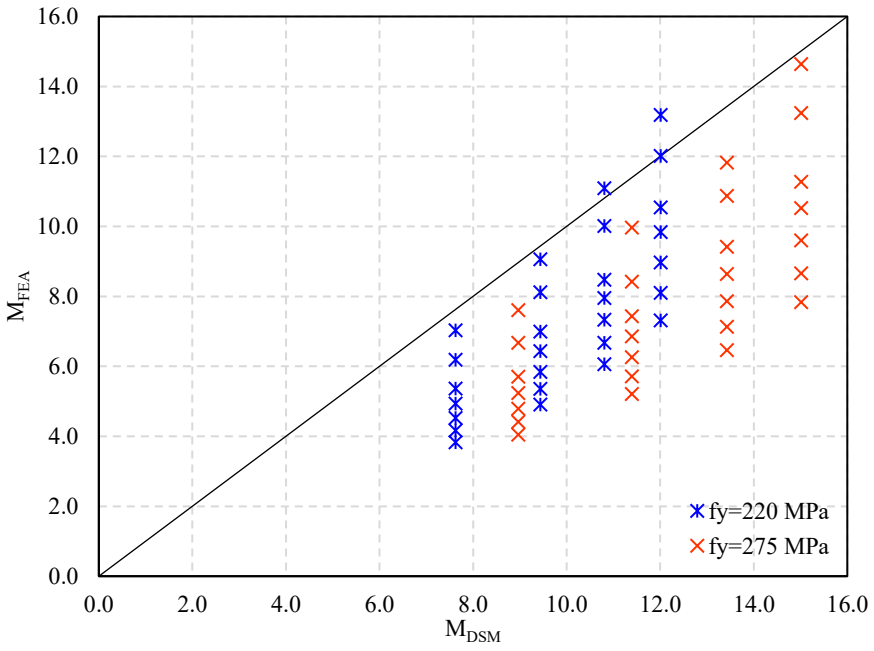

Fig. 4.7 Comparison of reduced moment capacity between DSM and FEA (web depth = 150 mm)

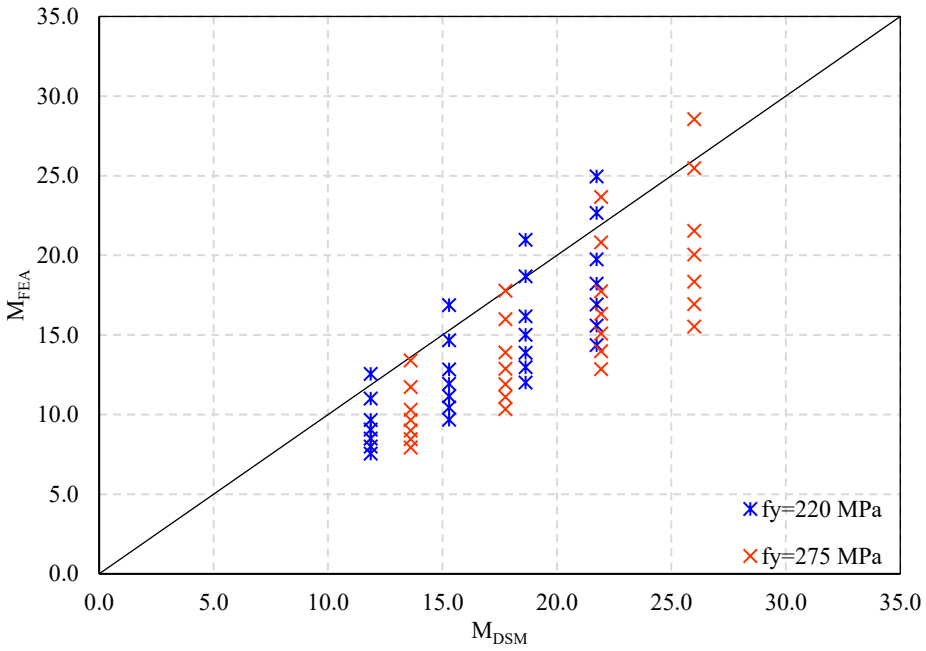

Fig. 4.8 Comparison of reduced moment capacity between DSM and FEA (web depth = 200 mm)

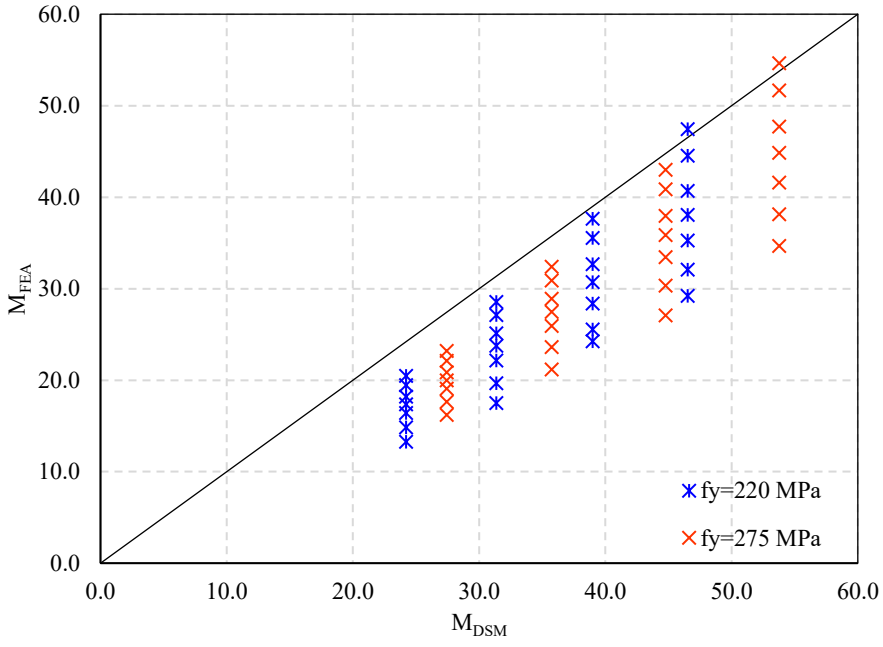

Fig. 4.9 Comparison of reduced moment capacity between DSM and FEA (web depth = 250 mm)

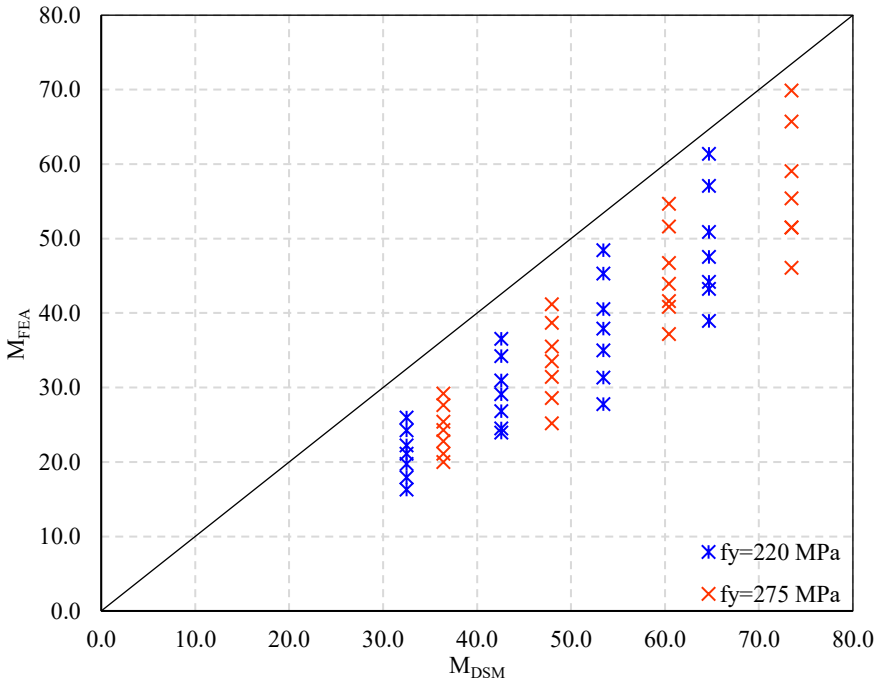

Fig. 4.10 Comparison of reduced moment capacity between DSM and FEA (web depth = 300 mm)

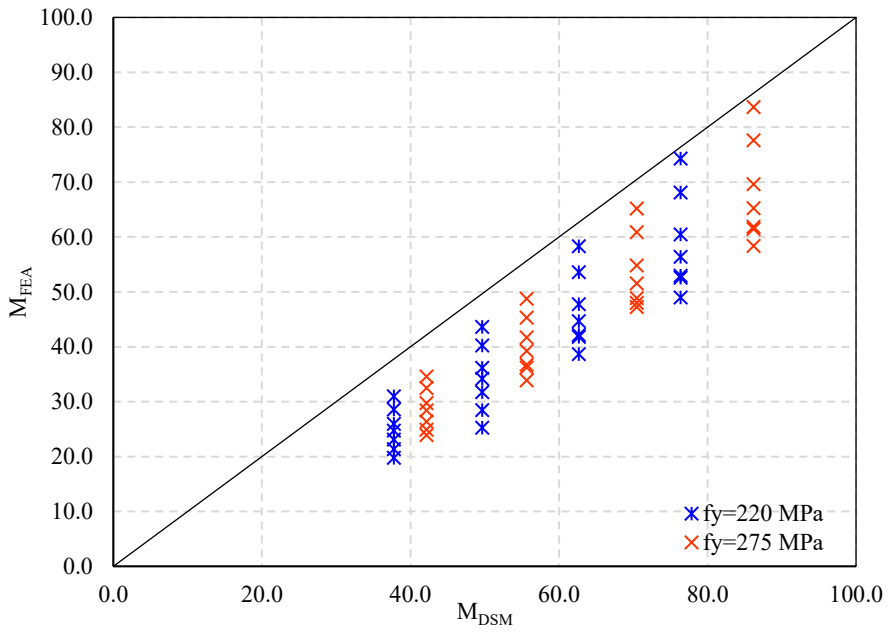

Fig. 4.11 Comparison of reduced moment capacity between DSM and FEA (web depth = 350 mm)

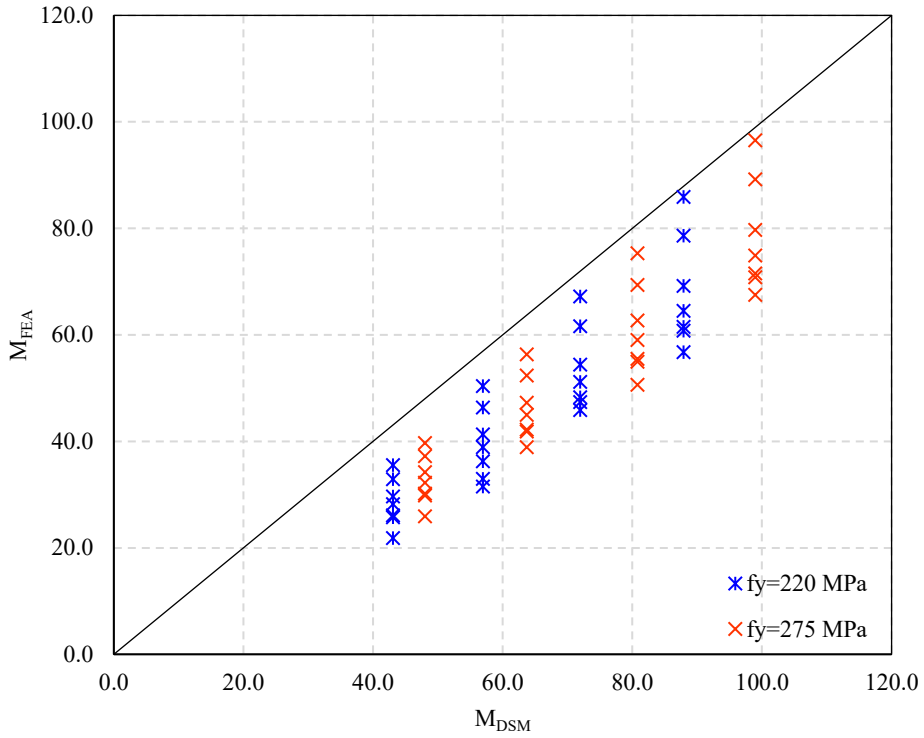

Fig. 4.12 Comparison of reduced moment capacity between DSM and FEA (web depth = 400 mm)

For bolt group 4×2:

The comparison between DSM and FEA results for a web depth of 150 mm yielded an R^2 value of 0.53, a mean bias of 1.59, and a coefficient of variation of 0.22. These results indicate that DSM predictions exhibit only a moderate correlation with the FEA data and generally overestimate the reduced moment capacities by approximately 59%. For a web depth of 200 mm, the analysis produced an R^2 value of 0.74, a mean bias of 1.19, and a coefficient of variation of 0.16. This suggests a good correlation between the two methods, with DSM overestimating the reduced moment capacities by around 19%.

The comparison for a web depth of 250 mm yielded an R^2 value of 0.70, a mean bias of 1.39, and a coefficient of variation of 0.20. These results also demonstrate moderate correlation between the DSM and FEA moment capacities, with DSM overpredicting the strength by approximately 39%. Similarly,

for a web depth of 300 mm, the correlation between FEA and DSM predictions is moderate, with an average bias of 1.56, an R^2 value of 0.76, and a coefficient of variation of 0.23. These values indicate DSM overestimating the FEA strength by around 56%.

For a web depth of 350 mm, an R^2 value of 0.77, a mean bias of 1.41, and a coefficient of variation of 0.19 are obtained, also indicate good agreement between the FEA and DSM predictions. Though, DSM overpredicts the reduced moment capacity by 41% Finally, for a web depth of 400 mm, the R^2 value was 0.79, the mean bias 1.31, and the coefficient of variation 0.18. Here, DSM overpredicts the reduced moment capacity by 31% but the correlation between FEA and DSM predictions remains good.

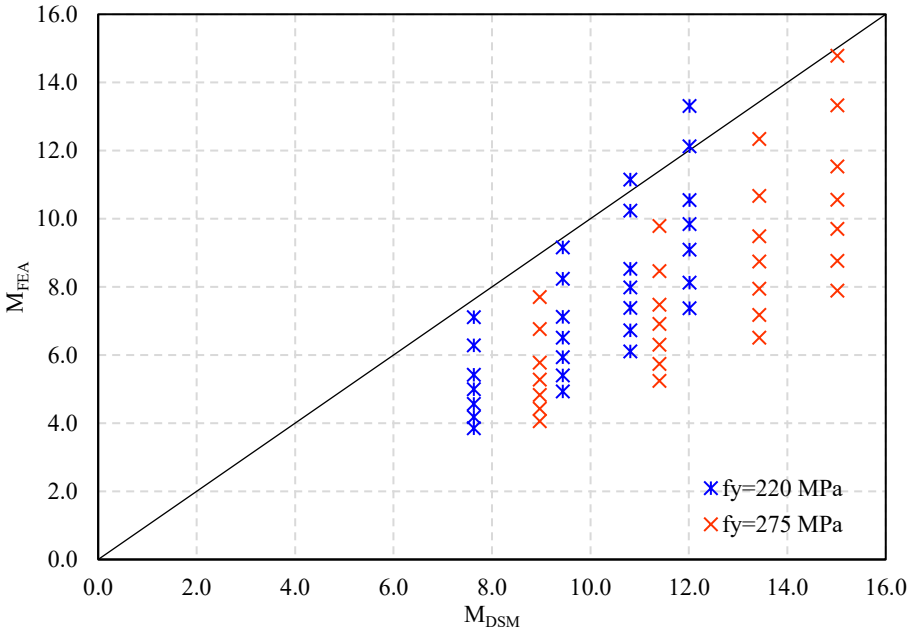

Fig. 4.13 Comparison of reduced moment capacity between DSM and FEA (web depth = 150 mm)

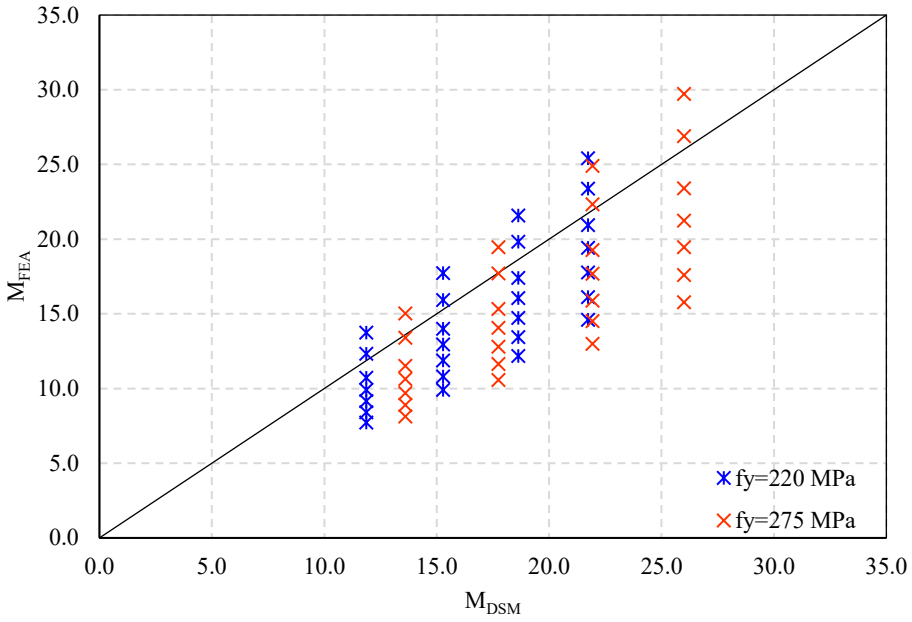

Fig. 4.14 Comparison of reduced moment capacity between DSM and FEA (web depth = 200 mm)

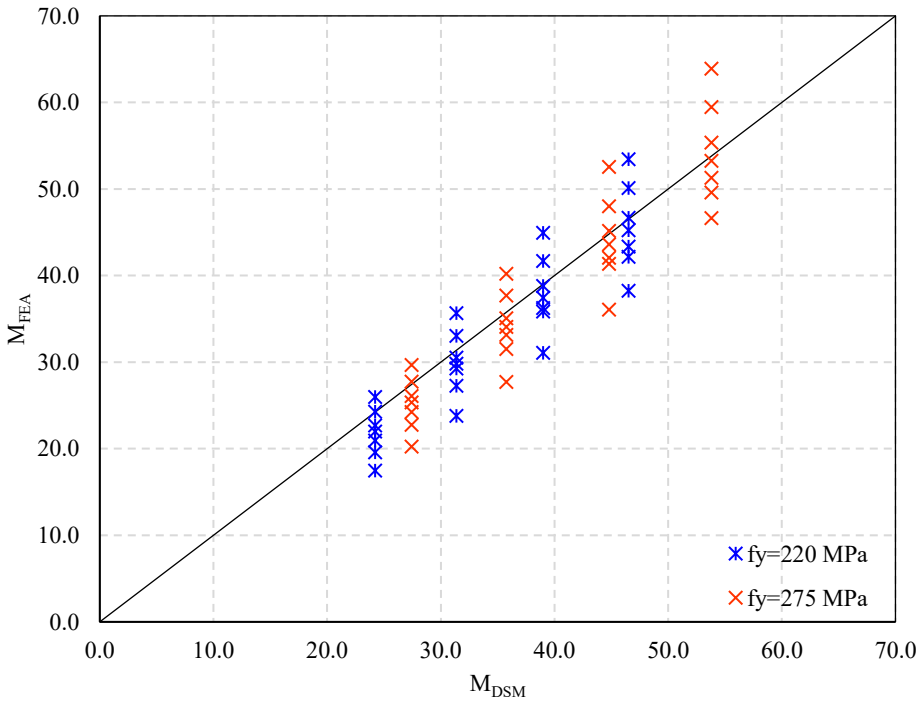

Fig. 4.15 Comparison of reduced moment capacity between DSM and FEA (web depth = 250 mm)

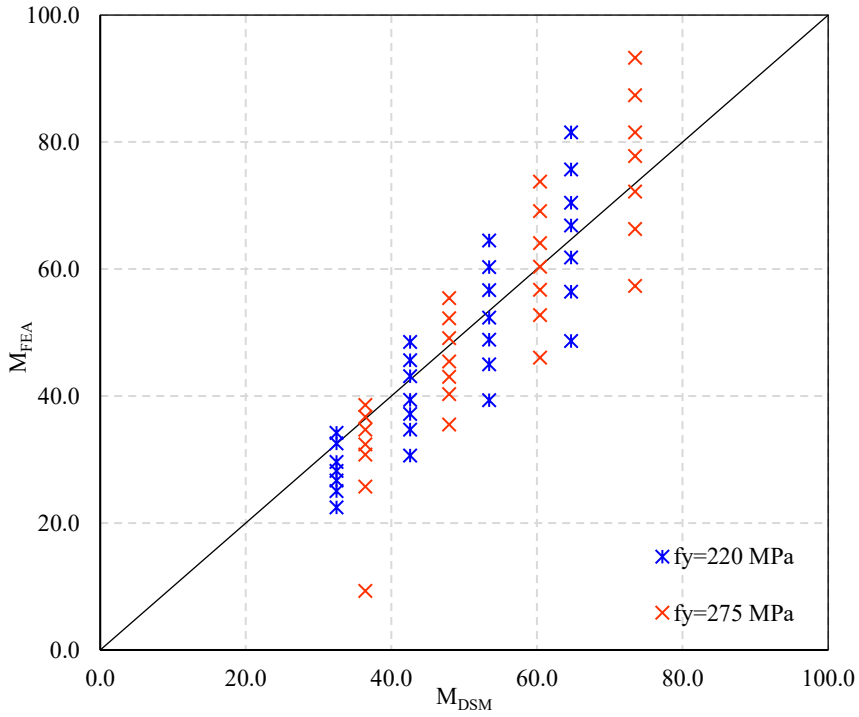

Fig. 4.16 Comparison of reduced moment capacity between DSM and FEA (web depth = 300 mm)

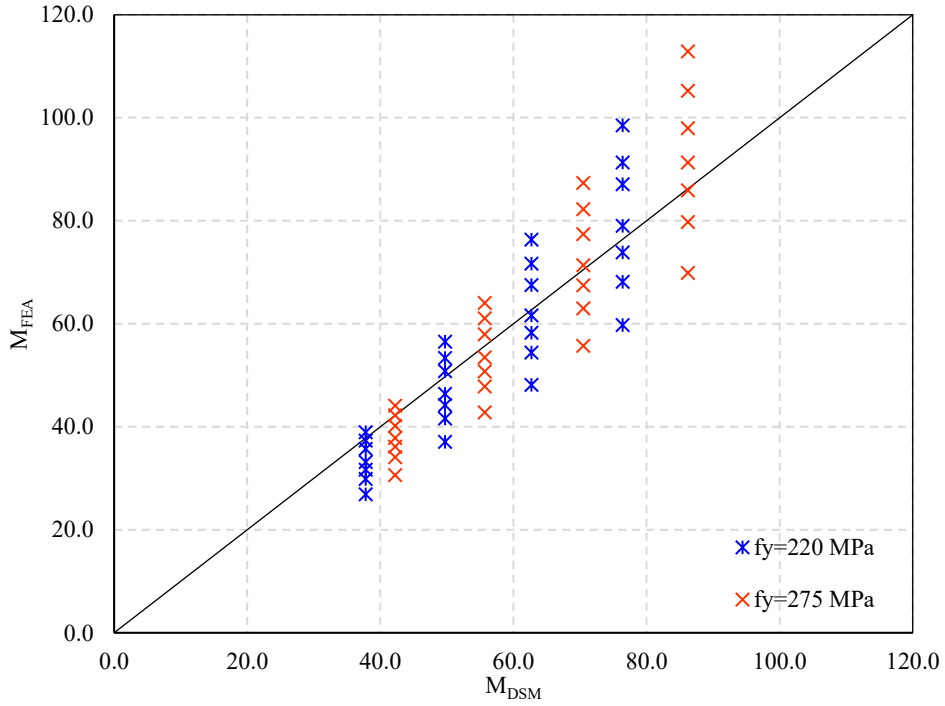

Fig. 4.17 Comparison of reduced moment capacity between DSM and FEA (web depth = 350 mm)

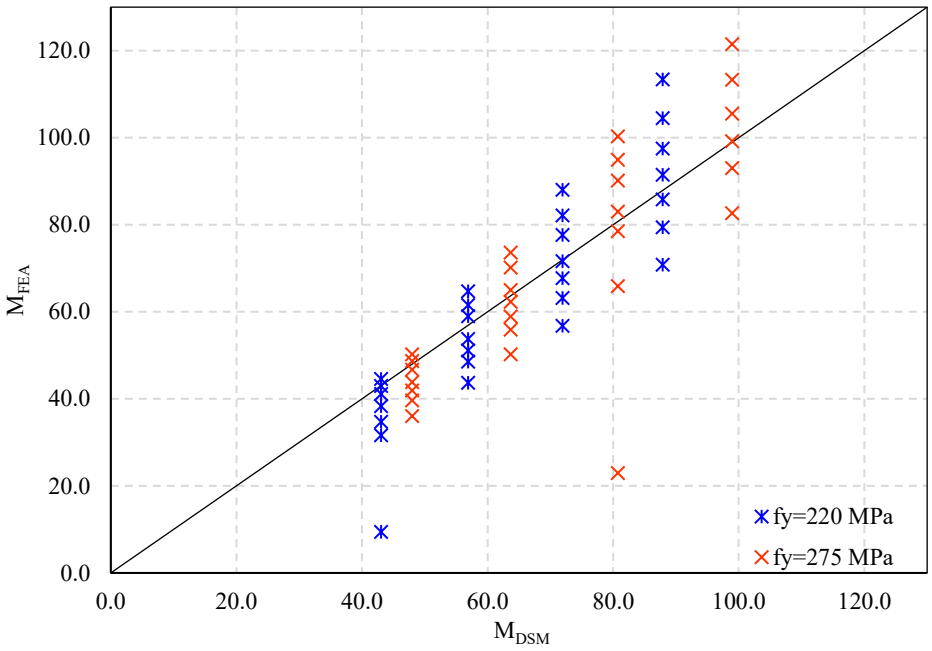

Fig. 4.18 Comparison of reduced moment capacity between DSM and FEA (web depth = 400 mm)

Table 4-1 shows summary of DSM and FEA comparison metrics for all bolt-group configurations across web depths

Bolt group	Depth (mm)	Mean bias	R^2	COV	Behaviour
2×2	150	1.54	0.49	0.22	Unconservative
	200	1.18	0.72	0.16	Unconservative
	250	1.60	0.78	0.26	Unconservative
	300	1.95	0.75	0.28	Unconservative
	350	1.72	0.77	0.24	Unconservative
	400	1.58	0.80	0.21	Unconservative
3×2	150	1.62	0.51	0.23	Unconservative
	200	1.20	0.73	0.17	Unconservative
	250	1.46	0.69	0.21	Unconservative
	300	1.63	0.74	0.25	Unconservative
	350	1.44	0.76	0.19	Unconservative
	400	1.36	0.78	0.18	Unconservative
4×2	150	1.59	0.53	0.22	Unconservative
	200	1.19	0.74	0.16	Unconservative
	250	1.39	0.70	0.20	Unconservative
	300	1.56	0.76	0.23	Unconservative
	350	1.41	0.77	0.19	Unconservative
	400	1.31	0.79	0.18	Unconservative

4.3 Comparison of FEA with Lim and Nethercot and Mojtabaei et al. [13], [12]

All graphs illustrate the comparative accuracy of different authors (Lim and Nethercot [13], and Mojtabaei et al. [12]) against finite element results for predicting the reduced moment capacity. The x-axis represents the existing ultimate moment capacity values predicted using formulas proposed by Lim & Nethercot [13] and Mojtabaei et al. [12] whereas the y-axis represents the ultimate moment capacity obtained from finite element analysis (FEA). There are two types of shapes used to illustrate the graph and a diagonal line shows perfect agreement, where the predicted ultimate moment capacity equals the

FEA ultimate moment capacity. From Figs. 4.19 – 4.24, it is shown that the value found from using equation of Lim and Nethercot [13] is closer to the diagonal line than using equation of Mojtabaei et al. [12]. But this scenario is observed for Lim and Nethercot [13] , when the moment capacity has lower value. Mojtabaei et al.[12] underestimates the reduced moment capacity for bolt group 2×2, while for bolt group 3×2 and 4×2 the moment capacities are closer to the diagonal line.

From Figs. 4.21 – 4.24, it is seen demonstrating that both analytical formulations provide reliable estimations when compared with FEA results for bolt group 3×2 and 4×2. However, the Lim and Nethercot [13] model exhibits closer alignment and reduced scatter, indicating better predictive performance for all bolt group.

For bolt group 2×2:

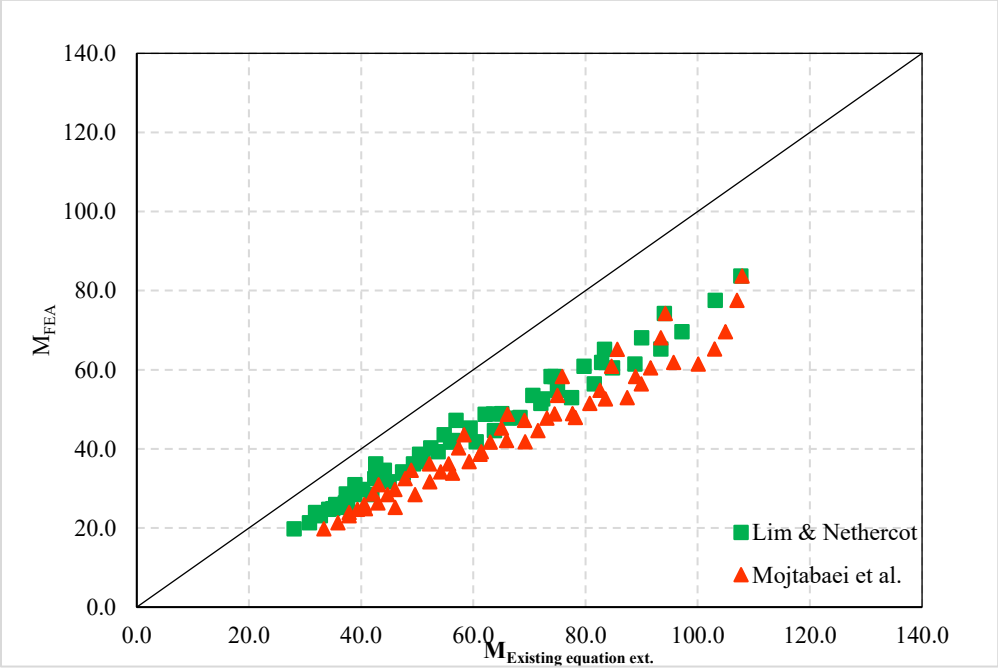

Fig. 4.19 Comparison of M_{FEA} with $M_{Existing\ equation\ ext.}$ (Web depth = 350 mm)

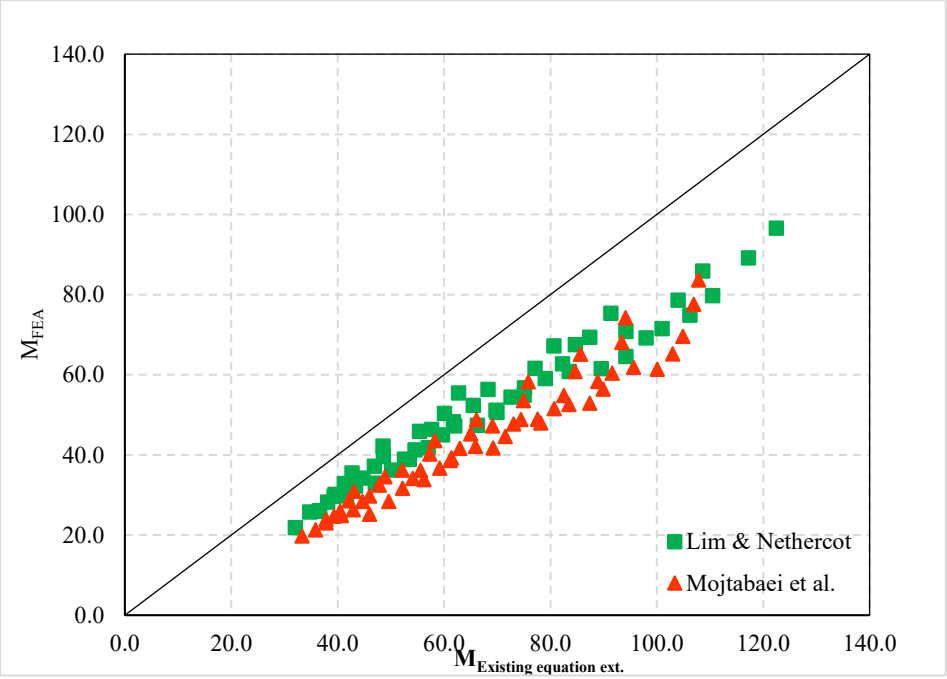

Fig. 4.20 Comparison of M_{FEA} with $M_{Existing\ equation\ ext.}$ (Web depth = 400 mm)

For bolt group 3x2:

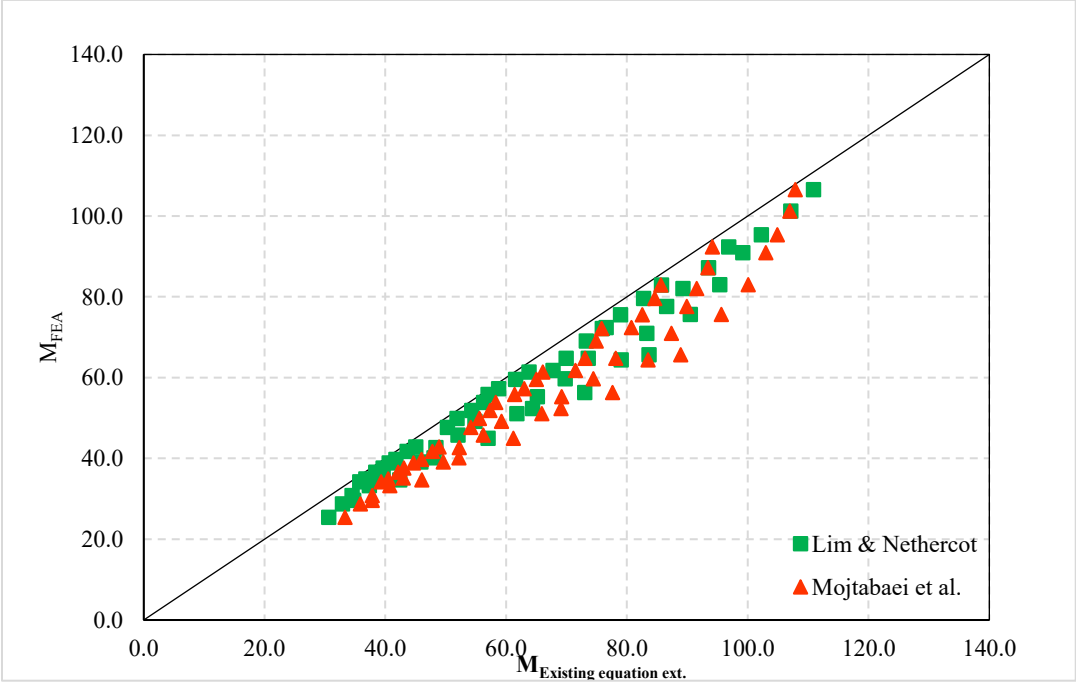

Fig. 4.21 Comparison of M_{FEA} with $M_{Existing\ equation\ ext.}$ (Web depth = 350 mm)

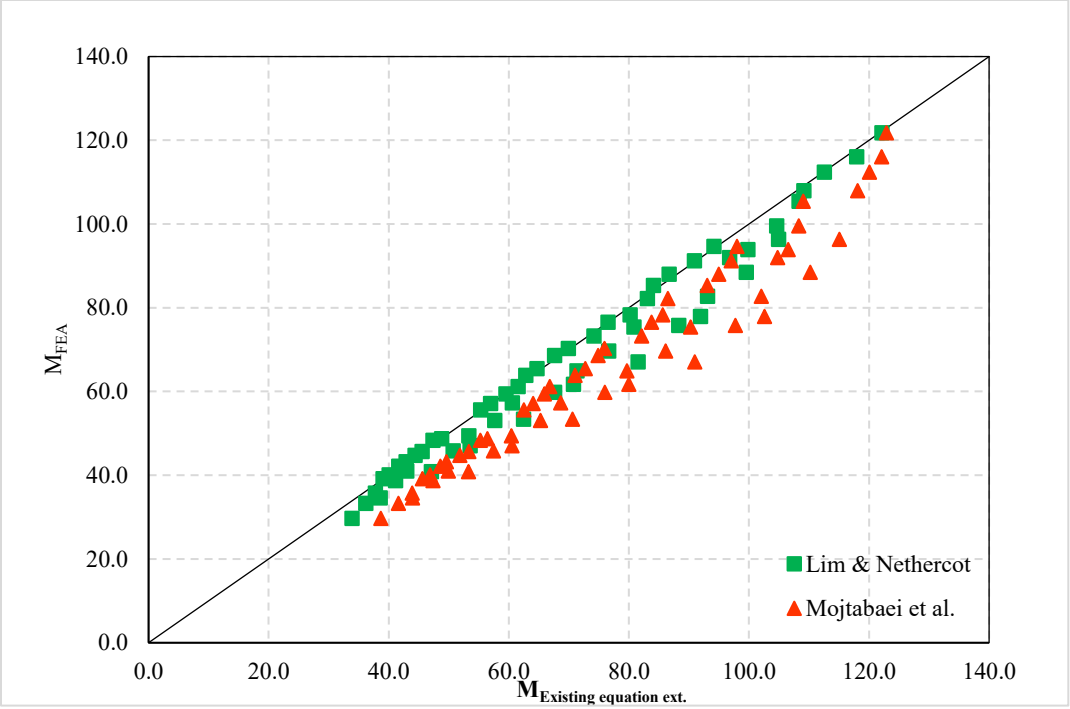

Fig. 4.22 Comparison of M_{FEA} with $M_{Existing\ equation\ ext.}$ (Web depth = 400 mm)

For bolt group 4x2:

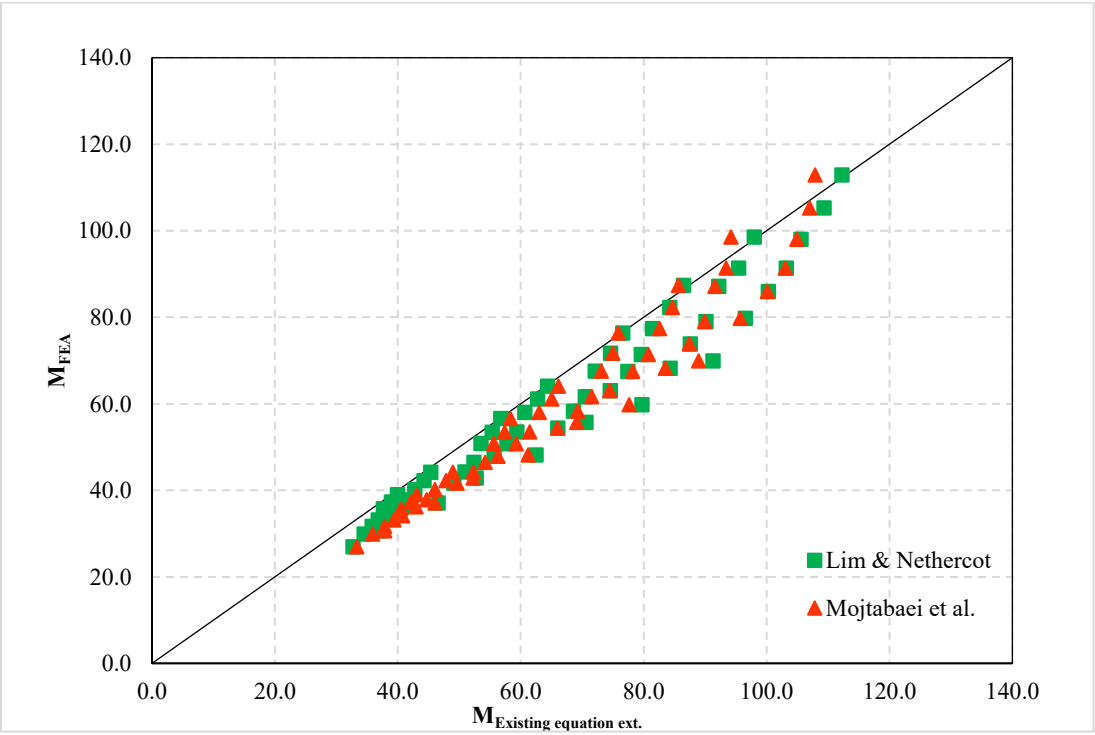

Fig. 4.23 Comparison of M_{FEA} with $M_{Existing\ equation\ ext.}$ (Web depth = 350 mm)

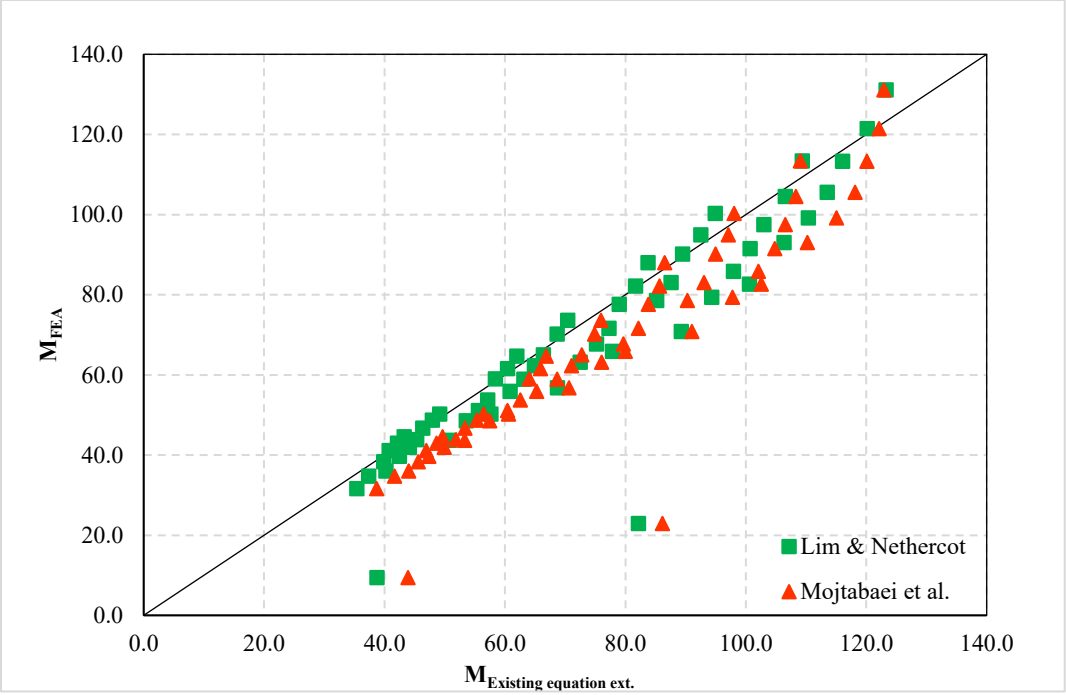

Fig. 4.24 Comparison of M_{FEA} with $M_{Existing\ equation\ ext.}$ (Web depth = 400 mm)

In this chapter, the formula used by Lim and Nethercot [13] and Mojtabaei et al. [12] are presented to determine the existing reduced moment capacity.

For Lim and Nethercot [13]

$$M_u^{ana} = M_u^{BS} \times (\alpha \ln(\frac{a_B}{D}) + \beta) \tag{4.7}$$

For Mojtabaei et al. [12]**:**

$$R = 1 - 0.42e^{(-13.8(t/X)(l_b/h))} \tag{4.8}$$

$$M_c = RM_u \tag{4.9}$$

It should be noted that the formulations proposed by Lim and Nethercot [13] and Mojtabaei et al. [12] were originally developed for CFS members. In this study, these equations are applied to CFA channel sections.

4.4 Proposed equation for reduced moment capacity of CFA

In the previous section, the reduced moment capacity is observed comparing with FEA and existing equation of Lim and Nethercot [13] and Mojtabaei et al. [12]. Although those existing equations have been widely applied in CFS connections, several limitations became evident when extended to CFA channel sections. Firstly, the equation proposed by Lim and Nethercot [13] demonstrates relatively good agreement with FEA results at lower capacity ranges; however, its accuracy diminishes at higher values. Moreover, the applicability of this formulation is limited by its calibration range, as it is valid only for a specific set of section slenderness ratios (D/t) and within a defined range of parameter values. Therefore, when using this equation to determine the ultimate moment capacity, data from all sections cannot be applied directly. Secondly, the equation presented by Mojtabaei et al. [12] is found to underestimate the ultimate moment capacity for smaller bolt groups (2×2), although it performs better for larger configurations (3×2 and 4×2). Nevertheless, this formulation also fails to incorporate the combined effects of shear bending interaction, which was clearly observed in the FEA results.

The original equation proposed by Lim and Nethercot [13] was developed based on experimental and numerical results for cold-formed steel sections, with specific calibration parameters (α and β) determined within their test range. However, when applied to CFA sections, the predicted reduced moment capacities showed noticeable deviations from the present FEA results. To improve the accuracy of prediction for CFA, the coefficients α and β of Lim and Nethercot [13] equations were recalibrated using the numerical results from six different sections web depth with varying D/t ratios. This modification ensures that the equation more accurately reflects the behaviour of CFA members across a broader range of slenderness values. In this study, the values of α and β are updated and given in Table 4-2.

So, the equation for the reduced moment capacity of CFA sections is

$$\frac{M_u^{ana}}{M_u^{BS}} = \alpha \ln(\frac{a_B}{D}) + \beta \tag{4.10}$$

The newly derived regression equations in this study reduced the overestimation to about 0.17%, indicating an improvement in prediction accuracy.

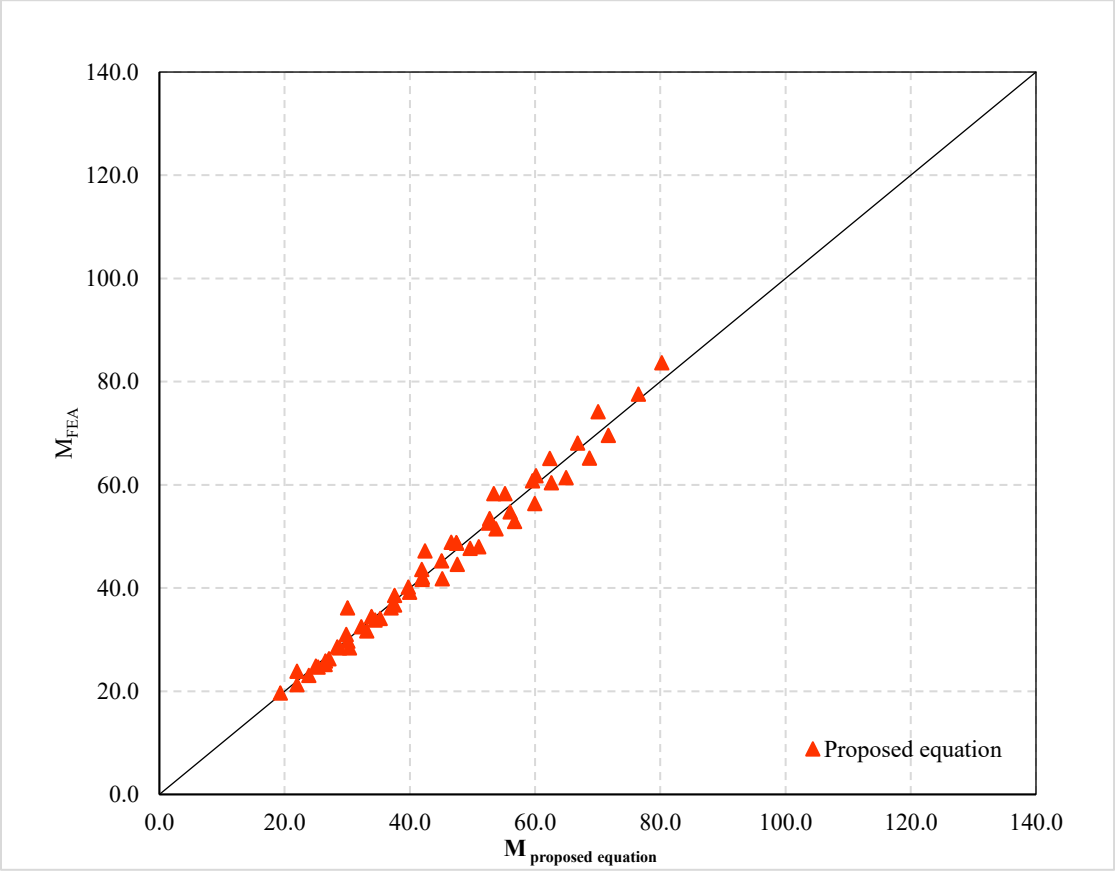

Fig. 4.25 Comparison of M_{FEA} with $M_{proposed\ equation.}$ (Web depth = 350 mm)

When the web depth was 400 mm, the new regression equations developed in this study reduced the error to only 0.5%, demonstrating a significant improvement in prediction accuracy.

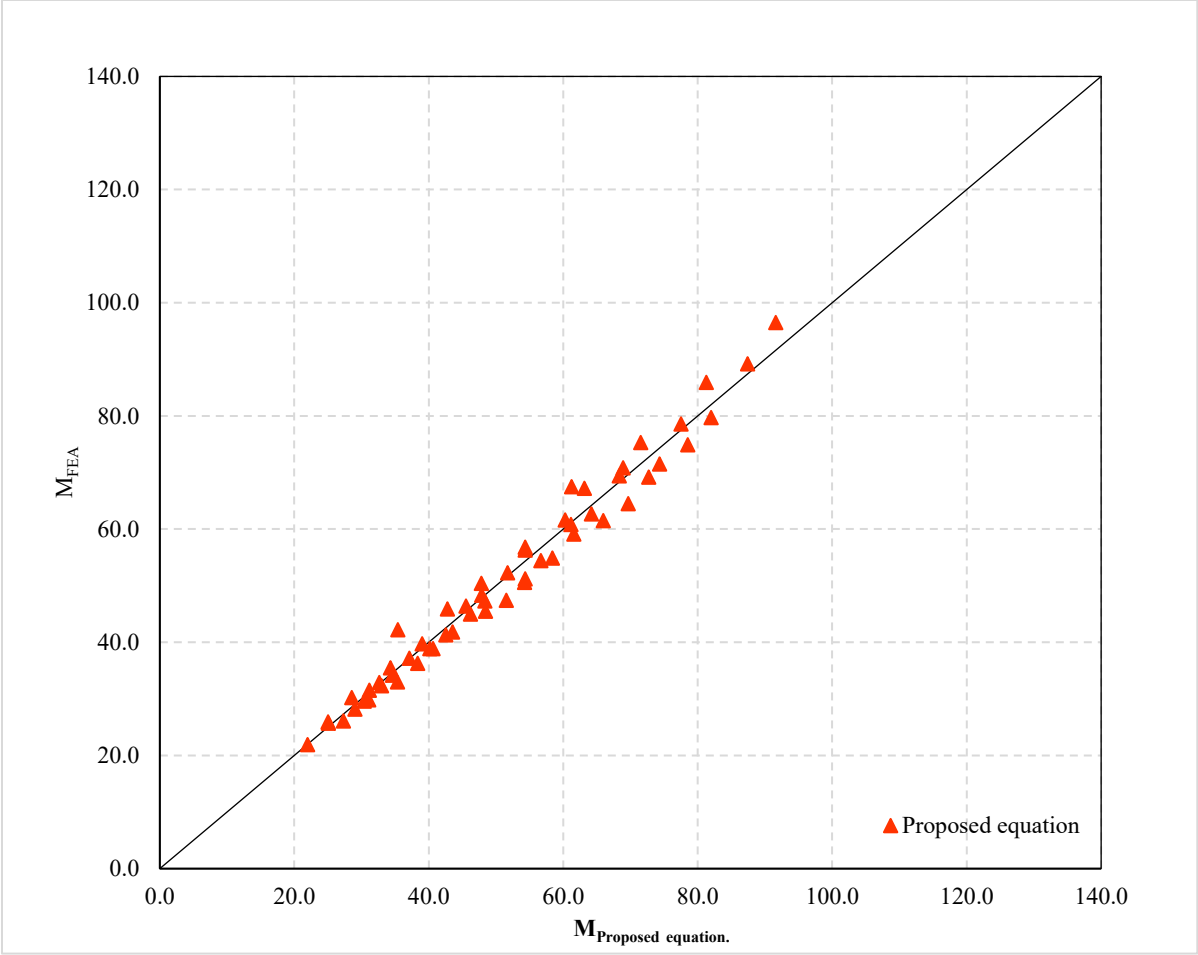

Fig. 4.26 Comparison of M_{FEA} with $M_{proposed\ equation.}$ (Web depth = 400 mm)

Table 4-2 Parameters of Equation 4.10

Depth, D (mm)	D/t	bolt-group array	α	β
150	60	2×2	0.2065	0.5273
		3×2	0.2283	0.5424
		4×2	0.2355	0.5473
	50	2×2	0.2434	0.5881
		3×2	0.2552	0.6022
		4×2	0.2561	0.6060
	42.86	2×2	0.2581	0.6449
		3×2	0.2705	0.6593
		4×2	0.2769	0.6640
	37.50	2×2	0.2932	0.7077
		3×2	0.2949	0.7204
		4×2	0.2968	0.7273
200	80	2×2	0.1904	0.5609
		3×2	0.2334	0.5964
		4×2	0.2427	0.6051
	66.67	2×2	0.2322	0.6285
		3×2	0.2684	0.6619
		4×2	0.2826	0.6642
	57.14	2×2	0.2723	0.6938
		3×2	0.2904	0.7181
		4×2	0.2959	0.7277
	50	2×2	0.2955	0.7494
		3×2	0.3055	0.7722
		4×2	0.3119	0.7829
250	100	2×2	0.1489	0.5859
		3×2	0.1791	0.7287
		4×2	0.1779	0.7458
	83.33	2×2	0.1814	0.6123
		3×2	0.2491	0.7259
		4×2	0.1784	0.7854
	71.43	2×2	0.2002	0.6637
		3×2	0.1901	0.8144
		4×2	0.1782	0.8359
	62.50	2×2	0.2191	0.7012

Depth, D (mm)	D/t	bolt-group array	α	β
250	62.50	3×2 4×2	0.1762 0.1719	0.8444 0.8598
300	120	2×2 3×2 4×2	0.1523 0.2032 0.1929	0.5460 0.7189 0.7355
	100	2×2 3×2 4×2	0.1717 0.2308 0.2228	0.5626 0.7407 0.7688
	85.71	2×2 3×2 4×2	0.1717 0.3022 0.2424	0.5821 0.7272 0.7876
	75	2×2 3×2 4×2	0.1776 0.2645 0.2622	0.6234 0.7929 0.8332
350	140	2×2 3×2 4×2	0.1468 0.1728 0.1683	0.5363 0.7039 0.7195
	116.67	2×2 3×2 4×2	0.1611 0.2078 0.2023	0.5574 0.7379 0.7609
	100	2×2 3×2 4×2	0.1429 0.2285 0.2295	0.5888 0.7511 0.7829
	87.50	2×2 3×2 4×2	0.1537 0.2397 0.2496	0.5983 0.7635 0.7986
400	160	2×2 3×2 4×2	0.1506 0.1657 0.1591	0.5361 0.7117 0.7284
	133.33	2×2 3×2 4×2	0.1528 0.1968 0.1925	0.5651 0.7479 0.7721
	114.29	2×2 3×2 4×2	0.1451 0.2159 0.2222	0.5909 0.7702 0.7986
	100	2×2 3×2 4×2	0.1528 0.2245 0.2398	0.6021 0.7787 0.8080

4.5 Reliability analysis

A reliability assessment was undertaken to determine the accuracy of the proposed formulae. The reliability analysis of the moment capacity predictions for CFA channel sections was evaluated using the Load and Resistance Factor Design (LRFD) approach. This method is commonly adopted in the development and calibration of American structural design standards and is incorporated in the Aluminium Design Manual (ADM) [66]. In 1979, Galambos evaluated the reliability index for limit states in the Specifications for Aluminum Structures.

$$\phi = \frac{1.521\, M_m F_m P_m}{exp\left(\beta\sqrt{\left\{V_R^2 + V_Q^2\right\}}\right)} \tag{4.11}$$

Using Equation 4.11, the reliability index for the aluminium channel sections was calculated as $\beta = 2.27$, which exceeds the target reliability index of $\beta = 2.18$ given in the ADM Commentary for a dead-to-live load ratio of 0.2. This confirms that the proposed design predictions provide an adequate and slightly conservative level of reliability.

4.6 Concluding remark

This chapter has covered the approach taken to model the apex joint of CFA portal frames using back-to-back channel sections in ABAQUS. Following the methodology of Lim and Nethercot [13], a single-channel section was modeled in ABAQUS. Each stage of the modelling process, from part creation, element and material selection, and spring idealizations to the application of boundary conditions and loading, was carefully chosen to reflect the structural behaviour observed in laboratory tests. The validation process showed that the finite element results closely matched the results of the experiments. This provides assurance that the FE models created are robust and sufficient for analyzing the CFA apex joints.

Chapter 5- Conclusion

This study has filled an important gap in the literature by investigating the ultimate moment capacity of bolted back-to-back CFA channel sections. Earlier CFA research focused mainly on full frames, axial compression, base and apex connections, but none of the existing studies looked at the moment capacity of back-to-back bolted joints. Although similar work has been done on CFS, those results cannot be applied directly to aluminium because the two materials behave differently. This research therefore provides the first detailed investigation of bolted connection type in back-to-back CFA channel sections.

A FE model was developed and its accuracy was confirmed by comparing it with reliable experimental results from the literature Lim and Nethercot [13]. Using the validated model, a parametric study was carried out. The analysis showed that premature web buckling near the bolted joint is the main factor that limits the moment capacity of back-to-back CFA channel sections. From these findings, a new prediction equation was developed to estimate the ultimate moment capacity of the joint. A reliability analysis confirmed that the proposed equation meets accepted safety requirements.

Overall, this thesis provides new and practical knowledge on the behaviour of bolted CFA connections. The findings support the broader use of CFA as a lightweight, corrosion-resistant alternative to steel, especially in coastal and aggressive environments.

In Summary, the original contributions of this thesis are summarised as follows:

1. Development of the first numerical modelling framework for back-to-back CFA channel sections with bolted joints.
2. Execution of the first detailed parametric study on the moment capacity of CFA apex joints.

3. Proposal of the first design equation for predicting the reduced moment capacity of CFA joints.
4. Quantification of the unconservatism of DSM when applied to CFA members with bolted joints.
5. Reliability calibration of the proposed design formula, demonstrating that it achieves an adequate and slightly conservative level of reliability consistent with aluminium design provisions.

Based on the findings of this study and previous research, some future works are identified:

1. Future studies should include full-scale experimental testing of CFA back-to-back channel apex joints to validate the proposed equation under realistic aluminium-specific failure mechanisms such as lower elastic modulus, different post-yield behaviour, and strain hardening effects.
2. Numerical investigations should incorporate more explicit bolt modelling strategies. This includes modelling bolt bearing deformation, and initial slip due to bolt hole clearance.
3. The scope of the investigation should be extended beyond apex joints to include CFA eaves joints. Studying these joints would enable a more complete understanding of connection performance.
4. Future work may incorporate nonlinear strain hardening models for aluminium alloys to better capture post-yield behaviour, particularly for stocky sections where buckling may not govern immediately.
5. Finally, future research should extend the validated CFA joint models to the analysis of full portal frame systems.

Reference

[1] W. S. Miller, L. Zhuang, J. Bottema, A. J. Wittebrood, P. D. Smet, A. Haszler, and A. Vieregge, "Recent development in aluminium alloys for the automotive industry," Mater. Sci. Eng. A, vol. 280, no. 1, pp. 37–49, 2000, doi: 10.1016/S0921-5093(99)00674-7.

[2] E. Georgantzia, M. Gkantou, and G. S. Kamaris, "Aluminium alloys as structural material: A review of research," Eng. Struct., vol. 227, p. 111372, 2021, doi: 10.1016/j.engstruct.2020.111372.

[3] Z. Fang, K. Roy, J. Xu, Y. Dai, B. Paul, and J. B. P. Lim, "A novel machine learning method to investigate the web crippling behaviour of perforated roll-formed aluminium alloy unlipped channels under interior-two flange loading," J. Build. Eng., vol. 51, p. 104261, 2022, doi: 10.1016/j.jobe.2022.104261.

[4] Z. Fang, K. Roy, B. Chen, Z. Xie, J. Ingham, and J. B. P. Lim, "Effect of the web hole size on the axial capacity of back-to-back aluminium alloy channel section columns," Eng. Struct., vol. 260, p. 114238, 2022, doi: 10.1016/j.engstruct.2022.114238.

[5] Z. Fang, K. Roy, J. M. Ingham, and J. B. P. Lim, "Assessment of end-two-flange web crippling strength of roll-formed aluminium alloy perforated channels by experimental testing, numerical simulation, and deep learning," Eng. Struct., vol. 268, p. 114753, 2022, doi: 10.1016/j.engstruct.2022.114753.

[6] K. Roy, B. Chen, Z. Fang, A. Uzzaman, and J. B. P. Lim, "Axial capacity of back-to-back built-up aluminium alloy channel section columns," J. Struct. Eng., vol. 148, no. 2, p. 04021265, 2022, doi: 10.1061/(ASCE)ST.1943-541X.0003240.

[7] K. Roy, B. Chen, Z. Fang, A. Uzzaman, X. Chen, and J. B. P. Lim, “Local and distortional buckling behaviour of back-to-back built-up aluminium alloy channel section columns,” Thin-Walled Struct., vol. 163, p. 107713, 2021, doi: 10.1016/j.tws.2021.107713.

[8] N. H. Pham, C. H. Pham, and K. J. Rasmussen, “Design of cold-rolled aluminium alloy channel beams subject to global buckling,” Thin-Walled Struct., vol. 180, p. 109885, 2022, doi: 10.1016/j.tws.2022.109885.

[9] D. P. McCrum, J. Simon, M. Grimes, B. M. Broderick, J. B. P. Lim, and A. M. Wrzesien, “Experimental cyclic performance of cold-formed steel bolted moment resisting frames,” Eng. Struct., vol. 181, pp. 1–14, 2019, doi: 10.1016/j.engstruct.2018.11.063.

[10] J. B. P. Lim, G. J. Hancock, G. C. Clifton, C. H. Pham, and R. Das, “DSM for ultimate strength of bolted moment-connections between cold-formed steel channel members,” J. Constr. Steel Res., vol. 117, pp. 196–203, 2016, doi: 10.1016/j.jcsr.2015.10.005.

[11] D. T. Phan, S. M. Mojtabaei, I. Hajirasouliha, T. L. Lau, and J. B. P. Lim, “Design and optimization of cold-formed steel sections in bolted moment connections considering bimoment,” J. Struct. Eng., vol. 146, no. 8, p. 04020153, 2020, doi: 10.1061/(ASCE)ST.1943.

[12] S. M. Mojtabaei, J. Becque, and I. Hajirasouliha, “Local buckling in cold-formed steel moment-resisting bolted connections: Behaviour, capacity, and design,” J. Struct. Eng., vol. 146, no. 9, p. 04020167, 2020, doi: 10.1061/(ASCE).

[13] J. B. P. Lim and D. A. Nethercot, “Ultimate strength of bolted moment-connections between cold-formed steel members,” Thin-Walled Struct., vol. 41, no. 11, pp. 1019–1039, 2003, https://doi.org/10.1016/S0263-8231(03)00045-4.

[14] S. M. Mojtabaei, J. Becque, and I. Hajirasouliha, “Behaviour and design of cold-formed steel bolted connections subjected to combined actions,” J. Struct. Eng., vol. 147, no. 4, p. 04021013, 2021, doi: 10.1061/(ASCE)ST.1943-541X.0002966.

[15] P. Kirk, “Design of a cold-formed section portal frame building system,” in Proc. Int. Specialty Conf. Cold-Formed Steel Structures, 1986, pp. 295–310. [Online]. Available: https://scholarsmine.mst.edu/isccss/8iccfss/8iccfss-session4/1

[16] K. F. Chung and L. Lau, “Experimental investigation on bolted moment connections among cold-formed steel members,” Eng. Struct., vol. 21, no. 10, pp. 898–911, 1999.

[17] F. Öztürk and S. Pul, “Experimental and numerical study on a full-scale apex connection of cold-formed steel portal frames,” Thin-Walled Struct., vol. 94, pp. 79–88, 2015, doi: 10.1016/j.tws.2015.04.004.

[18] J. Peng, J. Bendit, and H. B. Blum, “Experimental study of apex connection stiffness and strength of cold-formed steel double channel portal frames,” in Proc. 24th Int. Specialty Conf. Cold-Formed Steel Structures, 2018, pp. 547–565.

[19] H. B. Blum and K. J. R. Rasmussen, “Experimental and numerical study of connection effects in long-span cold-formed steel double channel portal frames,” J. Constr. Steel Res., vol. 155, pp. 480–491, 2019, doi: 10.1016/j.jcsr.2018.11.013.

[20] X. Zhang, K. J. R. Rasmussen, and H. Zhang, “Experimental investigation of locally and distortionally buckled portal frames,” J. Constr. Steel Res., vol. 122, pp. 571–583, 2016, doi: 10.1016/j.jcsr.2016.04.017.

[21] D. Dubbina, A. Stratan, A. Ciutina, and Z. Nagy, “Performance of ridge and eaves joints in cold-formed steel portal frames,” in Proc. Int. Specialty Conf. Cold-Formed Steel Structures, 2004, pp. 727–741.

[22] Y. B. Kwon, H. S. Chung, and G. D. Kim, “Experiments of cold-formed steel connections and portal frames,” J. Struct. Eng., vol. 132, no. 4, pp. 600–607, 2006, doi: 10.1061/ASCE0733-94452006132:4600.

[23] J. B. P. Lim and D. A. Nethercot, “F.E.-assisted design of the eaves bracket of a cold-formed steel portal frame,” Steel Compos. Struct., vol. 2, no. 6, pp. 411–428, 2002.

[24] H. B. Blum and K. J. R. Rasmussen, “Experimental investigation of long-span cold-formed steel double channel portal frames,” J. Constr. Steel Res., vol. 155, pp. 316–330, 2019, doi: 10.1016/j.jcsr.2018.11.020.

[25] J. B. P. Lim and D. A. Nethercot, “Finite element idealization of a cold-formed steel portal frame,” J. Struct. Eng., vol. 130, no. 1, pp. 78–94, 2004, doi: 10.1061/ASCE0733-94452004130:178.

[26] A. M. Wrzesien, J. B. P. Lim, Y. Xu, I. A. MacLeod, and R. M. Lawson, “Effect of stressed skin action on the behaviour of cold-formed steel portal frames,” Eng. Struct., vol. 105, pp. 123–136, 2015, doi: 10.1016/j.engstruct.2015.09.026.

[27] X. Zhang, K. J. R. Rasmussen, and H. Zhang, “Experimental investigation of locally and distortionally buckled portal frames,” J. Constr. Steel Res., vol. 122, pp. 571–583, 2016, doi: 10.1016/j.jcsr.2016.04.017.

[28] S. M. Mojtabaei, M. Z. Kabir, I. Hajirasouliha, and M. Kargar, “Analytical and experimental study on the seismic performance of cold-formed steel frames,” J. Constr. Steel Res., vol. 143, pp. 18–31, 2018, doi: 10.1016/j.jcsr.2017.12.013.

[29] D. P. McCrum, A. M. Wrzesien, J. Simon, M. Grimes, B. Broderick, and J. B. P. Lim, “Cyclic performance of cold-formed steel moment resisting frames,” ce/papers, vol. 2, no. 4, pp. 1837–1843, 2021, doi: 10.1002/cepa.1493.

[30] B. Paul, K. Roy, X. Chen, A. Shahmohammadi, I. Hajirasouliha, and J. B. P. Lim, “Simplified design method for cold-formed steel portal frames with back-to-back channel sections,” J. Constr. Steel Res., Advance Online Publication, 2025, doi: 10.1016/j.jcsr.2025.110077.

[31] ABAQUS Inc., ABAQUS/CAE User’s Guide, Version 6.21, Pawtucket, USA, 2021.

[32] E. Georgantzia, M. Gkantou, and G. S. Kamaris, “Aluminium alloys as structural material: A review of research,” Eng. Struct., vol. 227, 111372, 2021, doi: 10.1016/j.engstruct.2020.111372.

[33] G. De Matteis, G. Brando, and F. M. Mazzolani, “Pure aluminium: An innovative material for structural applications in seismic engineering,” Constr. Build. Mater., vol. 26, no. 1, pp. 677–686, 2012, doi: 10.1016/j.conbuildmat.2011.06.071.

[34] F. M. Mazzolani, “3D aluminium structures,” Thin-Walled Struct., vol. 61, pp. 258–266, 2012, doi: 10.1016/j.tws.2012.07.017.

[35] J.-H. Zhu, Z. Li, M. Su, and B. Young, “Design of aluminum alloy channel section beams,” J. Struct. Eng., vol. 146, no. 5, 2020, doi: 10.1061/(ASCE)ST.1943-541X.0002615.

[36] E. Georgantzia, M. Gkantou, G. S. Kamaris, and K. D. Kansara, “Design of aluminium alloy channel sections under minor axis bending,” Thin-Walled Struct., vol. 174, 109098, 2022, doi: 10.1016/j.tws.2022.109098.

[37] L. Yuan and Q. Zhang, “Design of aluminum alloy channel sections bent about the minor axis,” Structures, vol. 56, pp. 104889, 2023, doi: 10.1016/j.istruc.2023.104889.

[38] G. Sun, X.-Y. Sun, and J.-H. Fu, “Web crippling behaviour of high-strength aluminium alloy channel sections under concentrated loading: Numerical modelling and proposed design rules,” Buildings, vol. 13, no. 7, 1823, 2023, doi: 10.3390/buildings13071823.

[39] K. Jiang, B. Li, Y. Jing, A. Su, and O. Zhao, “Structural performance of aluminium alloy channel section tensile members connected with gusset plates,” Eng. Struct., vol. 333, 120177, 2025, doi: 10.1016/j.engstruct.2025.120177.

[40] L. A. T. Huynh, C. H. Pham, and K. J. R. Rasmussen, “Mechanical properties and residual stresses in cold-rolled aluminium channel sections,” Eng. Struct., vol. 199, 109562, 2019, doi: 10.1016/j.engstruct.2019.109562.

[41] A. McIntosh, K. Roy, J. B. P. Lim, and Z. Fang, “Web crippling of cold-formed carbon steel, stainless steel and aluminium sections: A comparative study,” Thin-Walled Struct., vol. 163, 107681, 2021, doi: 10.1016/j.tws.2021.107681.

[42] B. Paul, K. Roy, Y. Ji, Z. Fang, V. Sivaji, and J. B. P. Lim, “Moment capacity of perforated cold-formed aluminium channels – Tests, analysis, and design,” Thin-Walled Struct., vol. 204, 112261, 2024, doi: 10.1016/j.tws.2024.112261.

[43] N. H. Pham, C. H. Pham, and K. J. R. Rasmussen, “Global buckling capacity of cold-rolled aluminium alloy channel section beams,” J. Constr. Steel Res., vol. 179, 106521, 2021, doi: 10.1016/j.jcsr.2021.106521.

[44] N. H. Pham, C. H. Pham, and K. J. R. Rasmussen, “Member capacity of cold-rolled aluminium alloy channel columns – Part I: Experimental investigation,” Thin-Walled Struct., vol. 200, 111959, 2024, doi: 10.1016/j.tws.2024.111959.

[45] N. H. Pham, C. H. Pham, and K. J. R. Rasmussen, “Member capacity of cold-rolled aluminium alloy channel columns – Part II: Numerical investigation and design,” Thin-Walled Struct., vol. 200, 111960, 2024, doi: 10.1016/j.tws.2024.111960.

[46] Z. Fang, K. Roy, J. Xu, Y. Dai, B. Paul, and J. B. P. Lim, “A novel machine learning method to investigate the web crippling behaviour of perforated roll-formed aluminium alloy unlipped channels under interior-two flange loading,” J. Build. Eng., vol. 51, 104261, 2022, doi: 10.1016/j.jobe.2022.104261.

[47] Z. Fang, K. Roy, B. Chen, Z. Xie, and J. B. P. Lim, “Local and distortional buckling behaviour of aluminium alloy back-to-back channels with web holes under axial compression,” J. Build. Eng., vol. 47, 103837, 2022, doi: 10.1016/j.jobe.2022.103837.

[48] K. Roy, B. Chen, Z. Fang, A. Uzzaman, X. Chen, and J. B. P. Lim, “Local and distortional buckling behaviour of back-to-back built-up aluminium alloy channel section columns,” Thin-Walled Struct., vol. 169, 107713, 2021, doi: 10.1016/j.tws.2021.107713.

[49] K. Roy, Z. Fang, B. Chen, Z. Xie, and J. B. P. Lim, “Axial capacity of back-to-back built-up aluminum alloy channel section columns,” J. Constr. Steel Res., vol. 194, 107315, 2022, doi: 10.1016/j.jcsr.2022.107315.

[50] C. H. Pham, Behaviour and design of cold-rolled aluminium portal frame systems composed of back-to-back lipped channel sections, Ph.D. dissertation, Univ. of Sydney, 2021. [Online]. Available: https://ses.library.usyd.edu.au/handle/2123/25465

[51] H. C. Nguyen, C. H. Pham, and K. J. R. Rasmussen, “Experimental investigation of long-span cold-rolled aluminium built-up section portal frames: Braced columns and ultimate strength enhancement,” Eng. Struct., vol. 315, 118418, 2024, doi: 10.1016/j.engstruct.2024.118418.

[52] J. Liu, S. Chen, H. Li, D. Li, and X. Guo, “Experimental and numerical investigations on flexural behaviour of apex joints in aluminum alloy portal frames,” Structures, vol. 70, 107596, 2024, doi: 10.1016/j.istruc.2024.107596.

[53] H. C. Nguyen, C. H. Pham, and K. J. R. Rasmussen, “Experimental and numerical studies of base connections in cold-rolled aluminium built-up section portal frames,” Thin-Walled Struct., vol. 216, 113718, 2025, doi: 10.1016/j.tws.2025.113718.

[54] J. B. P. Lim, “Joint effects in cold-formed steel portal frames,” 2001.

[55] B. Paul, K. Roy, J. B. P. Lim, Z. Fang, K. McCollum, and D. Bell, “Moment-capacity of bolted side-plates for apex joint of nested tapered box beam portal frames,” J. Build. Eng., vol. 76, 107011, 2023, doi: 10.1016/j.jobe.2023.107011.

[56] B. Paul, K. Roy, Z. Fang, A. Shahmohammadi, and J. B. P. Lim, "Moment capacity of bolted-side plate for the eaves joint of nested tapered box beam portal frame," Int. J. Steel Struct., vol. 24, no. 5, pp. 1189–1201, 2024, doi: 10.1007/s13296-024-00888-7.

[57] A. Stratan, Z. Nagy, and D. Dubina, "Cold-formed steel pitched-roof portal frames of back-to-back plain channel sections and bolted joints," in Proc. Int. Specialty Conf. Cold-Formed Steel Struct., 2006, pp. 1189–1201. [Online]. Available: https://scholarsmine.mst.edu/cgi/viewcontent.cgi?article=1367&context=isccss

[58] Eurocode 9: Design of aluminium structures – Part 1-1: General structural rules, 1999.

[59] Aluminum Association, Aluminum Design Manual, Washington, DC, USA, 2020.

[60] K. F. Chung and L. Lau, "Experimental investigation on bolted moment connections among cold formed steel members," 1999. [Online]. Available: www.elsevier.com/locate/engstruct

[61] M. F. Wong and K. F. Chung, "Structural behaviour of bolted moment connections in cold-formed steel beam-column sub-frames," 2002. [Online]. Available: www.elsevier.com/locate/jcsr

[62] ABAQUS Inc., ABAQUS/CAE User's Guide, Version 6.21, Pawtucket, USA, 2021.

[63] B. W. Schafer and T. Peköz, "Computational modeling of cold-formed steel: characterizing geometric imperfections and residual stresses," 1998.

[64] AS/NZS 4600:2018, Cold-Formed Steel Structures, Standards Australia/Standards New Zealand, 2018.

[65] American Iron and Steel Institute (AISI), North American Specification for the Design of Cold-Formed Steel Structural Members, AISI S100-16, 2016.

[66] Aluminum Association, Aluminum Design Manual, Washington, DC, USA, 2020.

[67] Permalite Aluminium Building Solutions Pty Ltd., Permalite – Aluminium Roll-formed Purlin Solutions. Eagle Farm, Qld, Australia: BlueScope Lysaght, 2015.

[68] J. B. P. Lim and D. A. Nethercot, "Stiffness prediction for bolted moment-connections between cold-formed steel members," Journal of Constructional Steel Research, vol. 60, no. 1, pp. 85–107, Jan. 2004, doi: 10.1016/S0143-974X (03)00105-6.